BURLEIGH DODDS SERIES IN AGRICULTURAL SCIENCE

Achieving sustainable cultivation of oil palm

Volume 1: Introduction, breeding and cultivation techniques

Edited by Professor Alain Rival
Center for International Cooperation in Agricultural Research for Development (CIRAD), France

E-CHAPTER FROM THIS BOOK

burleigh dodds SCIENCE PUBLISHING

Modelling crop growth and yield in palm oil cultivation

Christopher Teh Boon Sung, Universiti Putra Malaysia, Malaysia; and
Cheah See Siang, Sime Darby Research Sdn. Bhd., Malaysia

1 Introduction

The first semi-mechanistic oil palm model was OPSIM (van Kraalingen, 1985). It was developed by taking into account some aspects of oil palm physiology and the physical processes and causal relationships between the environment and crop. OPSIM was modified by Gerristma (1988) in order to propose a more rigorous approach to estimate oil palm photosynthesis and later by Dufrêne et al. (1990), whose model (SIMPALM) relied much more on measured data of oil palm vegetative parameters. GPHOT, GPHOT2, OPLFSIM3 and later OPRODSIM (Henson, 1989, 2000, 2004, 2009) were the most comprehensive models at that period, as Henson's models progressively improved by including increasingly more effects and factors of oil palm growth and yield, including modelling the seasonal cycles of oil palm yield. Supplementary factors such as the effects of air vapour pressure deficit and available soil water on oil palm photosynthesis were also modelled. Fitted relationships, based

http://dx.doi.org/10.19103/AS.2017.0018.10

Chapter taken from: Rival, A. (ed.), *Achieving sustainable cultivation of oil palm Volume 1: Introduction, breeding and cultivation techniques*, Burleigh Dodds Science Publishing, Cambridge, UK, 2018, (ISBN: 978 1 78676 104 0; www.bdspublishing.com)

on measured data collected from various oil palm studies, were later included to better estimate oil palm root turnover, dry matter partitioning and flower sex ratios. Since then, the development of new oil palm models, such as WaNuLCAS (van Noordwijk et al., 2011), ECOPALM (Combres et al., 2013) and PALMSIM (Hoffmann et al., 2014) have increased in frequency. More recent oil palm models such as APSIM-Oil Palm (Huth et al., 2014), CLM-Palm (Fan et al., 2015) and CLIMEX-Oil Palm (Paterson et al., 2015) are actually components of a larger, more general modelling framework. The APSIM-Oil Palm, for instance, is one of the 30 sub-models for various crops, trees and pastures under the APSIM model framework.

The purpose of this chapter is to discuss the development of a new oil palm growth and yield model called PySawit. There are several key aspects that differentiate PySawit from other models. First, PySawit attempts to model oil palm photosynthesis in a more rigorous manner based on the biochemical photosynthesis model by Collatz et al. (1991), a modification of the original photosynthesis model by Farquhar et al. (1980). Other oil palm models tend to use oil palm's radiation use efficiency (based on Beer's law) to convert the intercepted radiation into gross photosynthesis. In our study, actual leaf measurements were done on young to mature palms to determine oil palm's Rubisco maximum capacity rate (V_{cmax}) and intercellular concentration of carbon dioxide (CO_2), both of which are needed to determine the leaf photosynthesis rate.

Second, the microclimate environment within and under the oil palm canopies is modelled by describing the soil–plant–atmosphere system as a network of resistances in which latent and sensible heat fluxes from the soil and crop must traverse, akin to the flow of electrical current, driven by potential differences and impeded by a series of resistances (Shuttleworth and Wallace, 1985). The Shuttleworth–Wallace (SW) evapotranspiration model is an important extension of the Penman–Monteith model (Monteith, 1965) as it allows the simultaneous heat fluxes from both soil and crop, unlike its predecessor that would only allow fluxes from either soil or crop but not both simultaneously. We further measured the relationship between oil palm's leaf stomatal conductance with photosynthetically active radiation (PAR) and air vapour pressure deficit (VPD), as these are needed to determine fluxes of latent heat and, thus, the amount of water loss from oil palm.

And third, PySawit is developed specifically for oil palm planted on a wide range of densities, from about 120 to 300 palms ha^{-1}. The recent oil palm models such as APSIM-Oil Palm, CLM-Palm and PALMSIM were validated only over a narrow planting density range of 127–156 palms ha^{-1}. The accuracy of the CLIMEX-Oil Palm, on the other hand, was not even validated. Moreover, most oil palm models, especially recent ones, have only been validated over a limited period of the oil palm growth stage (usually only when the palms have fully matured).

Consequently, the second purpose of this chapter is to discuss the evaluation of PySawit's accuracy when its predictions were compared with several measured parameters of growth and yield in oil palm aged 1–19 yrs. These oil palm were planted with 10 different planting densities, ranging from 122 to 296 palms ha^{-1}, in an oil palm estate at Merlimau, Malaysia. The degree of agreement between PySawit's predictions and observations was evaluated by visual inspection of scatterplots between predictions and observations and by the use of statistical goodness-of-fit indexes.

2 Theory and model development

PySawit simulations are for crop production level 2, where the growth and yield of oil palm are limited only by weather conditions and water availability (de Witt and Penning

de Vries, 1982). The model assumes that oil palm grows under optimal nutrient levels and without any detrimental effects from pests, diseases or weeds, and is managed by following standard practices (such as pruning and mulching) by the oil palm industry.

PySawit comprises five core components: 1) meteorology, 2) photosynthesis, 3) energy balance, 4) soil water and 5) crop growth. The meteorology component contains calculations pertaining to both daily and hourly meteorological elements such as air temperature, wind speed, humidity, solar irradiance and rain. The photosynthesis component calculates the oil palm photosynthesis rate, and the energy balance component deals with the various heat fluxes with the aim of determining the potential evapotranspiration and canopy temperature. The soil water component determines the soil water balance and the various water fluxes in the soil layers to estimate the amount of water available to the plant and the level of crop water stress, if any. The last component, crop growth, is aimed at estimating the crop maintenance, vegetative growth respirations and the bunch production and yield.

3 Modelling meteorology

Simulations begin with the meteorology component. PySawit requires only four daily meteorological parameters: minimum and maximum air temperature (°C), wind speed (m s^{-1}) and rain (mm) to estimate the various instantaneous meteorological properties such as solar irradiance, wind speed, air temperature, vapour pressure and humidity. Routine information on the site's local solar hours of sunrise t_{sr} and sunset t_{ss}, day length *DL* (hours), solar inclination θ (solar angle from vertical) (radians), extraterrestrial solar irradiance I_{et} (W m^{-2}), relative humidity *RH* (%) and saturated vapour pressure (mbar) was obtained from the work of Goudriaan and van Laar (1994).

Instantaneous total solar irradiance comprises two components: direct and diffuse components, where the direct component arrives from a single direction (the solar position), whereas the diffuse component arrives from all directions due to scattering and reflection from various surfaces in the environment. Calculations from Liu and Jordan (1960) were used to determine these solar radiation components as

$$I_t = I_{dr} + I_{df} \tag{1a}$$

$$I_{dr} = I_{et} \cdot \tau^m \tag{1b}$$

$$I_{df} = 0.3\left(1-\tau^m\right)I_{et} \tag{1c}$$

where I_t, I_{dr} and I_{df} are the instantaneous total, direct and diffuse solar irradiance, respectively (all in W m^{-2}); τ is the sky clearness index (or atmospheric transmittance, the ratio between I_t and I_{et}); and m is the optical mass number. The optical mass number m is determined from Campbell and Norman (1998) as

$$m = P_a / \left(101.3 cos\theta\right) \tag{2}$$

where P_a is the atmospheric pressure (kPa), assumed constant at 101 kPa.

Dimas et al. (2011) showed that τ can be estimated from relative humidity (*RH*) and in turn be used to calculate I_t and its components: I_{dr} and I_{df}. Hourly meteorological data for years 2015 and 2016 were obtained from weather stations located at five Malaysian

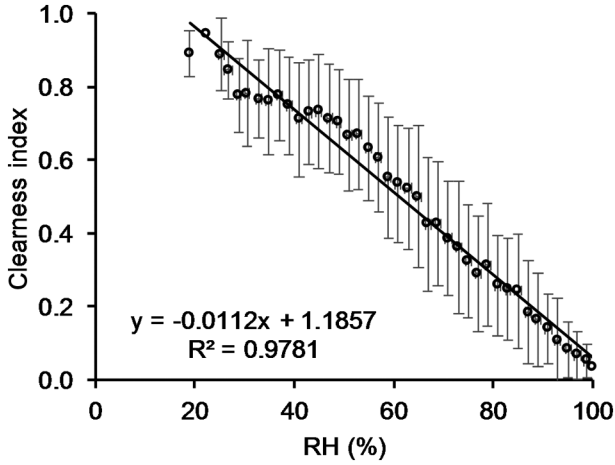

Figure 1 Linear relationship between measured relative humidity (*RH*) and sky clearness index between 2015 and 2016 for five stations located in Malaysia (N = 25548). Note: the bars represent one standard deviation.

oil palm estates: Bukit Selarong, Kedah (5.462824°N, 100.597084°E); Diamond Jubilee, Melaka (2.33333°N, 102.483333°E); Imam, Sabah (4.333333°N, 117.833333°E); Seri Intan, Perak (3.976583°N, 100.9739°E); and Ulu Remis, Johor (1.827778°N, 103.461944°E), where the following linear relationship between τ and relative humidity (RH) was derived:

$$\tau = 1.1857 - 0.0112RH \tag{3}$$

where *RH* (%) (Fig. 1).

The daily trend of instantaneous air temperature for the considered stations was also observed to vary sinuously with time during the period between 1.5 hours after the time of minimum air temperature and time of sunset. Outside this period, air temperature was observed to change linearly with time. This trend can be accurately depicted by the following mathematical relationships according to Wilkerson et al. (1983) as

$$T_a = \begin{cases} T_{set} + \dfrac{(T_{min} - T_{set})(24 + t_h - t_{ss})}{(t_{sr} + 1.5) + (24 - t_{ss})} & t_h < (t_{sr} + 1.5) \\ T_{set} + \dfrac{(T_{min} - T_{set})(t_h - t_{ss})}{(t_{sr} + 1.5) + (24 - t_{ss})} & t_h > t_{ss} \\ T_{min} + (T_{max} - T_{min}) sin\left[\dfrac{\pi(t_h - t_{sr} - 1.5)}{t_{ss} - t_{sr}}\right] & otherwise \end{cases} \tag{4a}$$

$$T_{set} = T_{min} + (T_{max} - T_{min}) sin\left[\frac{\pi(t_{ss} - t_{sr} - 1.5)}{t_{ss} - t_{sr}}\right] \tag{4b}$$

where T_a is the air temperature; T_{min} and T_{max} are the minimum and maximum air temperature, respectively; and T_{set} is the air temperature at the time of sunset (t_{ss}). All temperatures are in °C.

The dew point temperature T_{dew} for these five stations were rather constant throughout the year, with a mean of 23°C. This value is within the range reported by Mohd. Desa and Rakhecha (2006), who also observed a rather constant dew point temperature between 20°C and 24°C for 24 towns across Malaysia for the 1994 and 2003 periods.

Knowing the dew point temperature, T_{dew}, enables the determination of air vapour pressure according to Ephrath et al. (1996) as follows:

$$e_a = 6.1078 exp\left(\frac{17.269 T_{dew,cal}}{T_{dew,cal} + 237.3}\right) \tag{5}$$

where e_a is the air vapour pressure (mbar) and $T_{dew,cal}$ is the calibrated dew point temperature (°C), where it should be lower than the current air temperature, T_a:

$$T_{dew,cal} = MIN\left[\!\left[T_a,\ T_{dew}\right]\!\right] \tag{6}$$

where $MIN\left[\!\left[n_1, n_2, \ldots, n_n\right]\!\right]$ is the minimum function, returning the smallest of the enclosed values.

The instantaneous wind speed typically varies sinuously within the day as

$$u = MAX\left[\!\left[u_{min},\ u_{min} + \left(u_{max} - u_{min}\right) sin\left[\frac{\pi}{DL}\left(t_h - t_{sr} - 1.5\right)\right]\right]\!\right] \tag{7}$$

where u is the wind speed (m s^{-1}); u_{max} and u_{min} are the maximum and minimum wind speed for the day, respectively (m s^{-1}); and $MAX\left[\!\left[n_1, n_2, \ldots, n_n\right]\!\right]$ is the maximum function, returning the largest of the enclosed values. The mean daily minimum and maximum wind speed can be estimated by the following equations, developed by fitting the best function to the measured hourly wind speed data for several towns in Malaysia from 1982 to 1991 (Sopian et al., 1995):

$$u_{min} = 0.5591 u_d^{1.25} \tag{8}$$

$$u_{max} = 1.7976 u_d^{0.75} \tag{9}$$

where u_d is the mean daily wind speed (m s^{-1}).

4 Modelling photosynthesis

The photosynthesis model by Collatz et al. (1991), which is based on Farquhar et al. (1980), was adapted in order to determine the amount of CO_2 assimilated by the oil palm canopy, where gross leaf CO_2 assimilation is limited by the lowest of the three potential assimilation rates due to Rubisco, light and sink:

$$\Lambda_{sl/sh} = MIN\left[\!\left[v_c,\ v_{q,sl/sh},\ v_s\right]\!\right] \tag{10}$$

where $\Lambda_{sl/sh}$ is the gross leaf CO_2 assimilation rate for either sunlit (subscript *sl*) or shaded (*sh*) leaves, and v_c, v_q and v_s are the Rubisco-, light- and sink-limited assimilation rates, respectively. All assimilation rates are in μmol CO_2 m^{-2} leaf s^{-1}.

Leaf CO_2 assimilation rate is scaled up to canopy level, following Campbell and Norman (1998), by

$$\Lambda_{canopy} = \Lambda_{sl} L_{sl} + \Lambda_{sh} L_{sh} \tag{11}$$

where Λ_{canopy} is the gross canopy CO_2 assimilation rate (μmol CO_2 m^{-2} ground s^{-1}) and L_{sl} and L_{sh} are the sunlit and shaded leaf area indexes, respectively (both in m^2 leaf m^{-2} ground).

Equation 11 is integrated over sunrise (t_{sr}) to sunset (t_{ss}) to determine the daily gross canopy photosynthesis rate as

$$\Lambda_{canopy,d} = \frac{1.08}{PD} \int_{t_{sr}}^{t_{ss}} \Lambda_{canopy} dt \tag{12}$$

where $\Lambda_{canopy,d}$ is the daily gross photosynthesis rate (converted to kg CH_2O $palm^{-1}$ day^{-1}); and *PD* is the planting density (palms ha^{-1}). Integration is performed by the numerical Gaussian integration method, where five points over the diurnal period (from sunrise to sunset) are selected, and for each selected hour, the gross canopy CO_2 assimilation rate is calculated (Teh, 2006).

The following sub-sections describe the meaning and calculations of the various parameters in Eq. 10 and 11.

4.1 Rubisco-limited assimilation (v_c)

Rubisco-limited leaf CO_2 assimilation rate v_c is determined by

$$v_c = \frac{V_{cmax}\left(C_i - \Gamma^*\right)}{K_c\left(1 + O_a / K_o\right) + C_i} \tag{13}$$

where K_c is the Michaelis–Menten constant for CO_2 (μmol CO_2 mol^{-1} air); K_o is the Michaelis–Menten constant for O_2 (μmol O_2 mol^{-1} air); Γ^* is the CO_2 compensation point (μmol CO_2 mol^{-1} air); O_a is the ambient O_2 concentration in air (210 000 μmol O_2 mol^{-1} air); C_i is the intercellular CO_2 concentration (μmol CO_2 mol^{-1} air); and V_{cmax} is the maximum Rubisco capacity rate (μmol CO_2 m^{-2} leaf s^{-1}). The CO_2 compensation point Γ^* (CO_2 concentration at the point where assimilation is zero) is determined by

$$\Gamma^* = 0.5 O_a / \tau \tag{14}$$

where τ is the CO_2/O_2 specificity factor (μmol O_2 μmol^{-1} CO_2). For C3 plants like oil palm, τ indicates the level of competition between O_2 and CO_2 substrates for the Rubisco enzyme.

Most of the parameters in Eq. 13 are temperature-dependent and must be corrected for foliage temperature (T_f). Correction is made by multiplying their values at 25°C with their corresponding Q_{10} temperature coefficients (Table 1). Q_{10} is a measure of the rate of change of a given biochemical activity due to the increase in the temperature by 10°C.

Temperature correction for these parameters follows this general form:

$$\xi = \xi_{(25)} \times Q_{10,\xi}^{(T_f - 25)/10} \tag{15}$$

where $\xi_{(25)}$ is the parameter value at 25 °C, T_f is the canopy temperature (°C) and $Q_{10,\xi}$ is the relative change in parameter ξ for every 10 °C change (Table 1). However, V_{cmax} has to be additionally corrected for foliage temperatures greater than 40°C, after which the Rubisco enzyme degrades, causing a rapid decline in CO_2 assimilation:

Table 1 Values of temperature-dependent photosynthesis parameters $\xi_{(25)}$ at 25 °C. Except for $V_{cmax(25)}$, all values are from Bernacchi et al. (2001, 2002), and they are general values for C3 plants

$\xi_{(25)}$	Description	Unit	Value	$Q_{10,\xi}$
$K_{c(25)}$	Michaelis–Menten constant for CO_2	μmol CO_2 mol^{-1} air	270	2.786
$K_{o(25)}$	Michaelis–Menten constant for O_2	μmol O_2 mol^{-1} air	165000	1.355
$\tau_{(25)}$	CO_2/O_2 specificity factor	μmol O_2 μmol^{-1} CO_2	2800	0.703
$V_{cmax(25)}$	Maximum Rubisco capacity rate	μmol CO_2 m^{-2} leaf s^{-1}	79	2.573

$$V_{cmax} = \frac{V_{c\max(25)} \times 2.573^{(T_f - 25)/10}}{1 + exp\left[0.29\left(T_f - 40\right)\right]} \tag{16}$$

$V_{cmax(25)}$ for oil palm is determined to decline with tree age, from a mean (± s.e.) of 91.1 (±3.7) to 69.8 (±2.6) μmol CO_2 $m-^2$ leaf s^{-1} between palm ages 1 and 19 yrs (Fig. 2). The relationship between oil palm $V_{cmax(25)}$ and tree age can be described by the following linear equation:

$$V_{cmax(25)} = 87.935 - 0.0026age \tag{17}$$

where *age* refers to the tree age (in days).

Our measured $V_{cmax(25)}$ is between 10% and 30% smaller than that used by Fan et al. (2015) for their oil palm growth simulations. Fan et al. (2015) used a constant $V_{cmax(25)}$ of

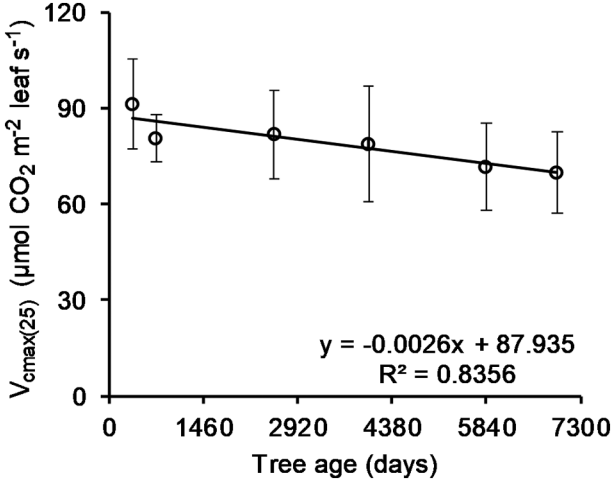

Figure 2 Changes in the maximum Rubisco capacity rate $V_{cmax(25)}$ with oil palm tree age. Leaf gas exchanges for 1- to 19-year-old palm trees were measured (N = 138) (Long and Bernacchi, 2003) using the TPS-2 Portable Photosynthesis System (PP Systems International, Inc., Amesbury, US), and based on the gas exchange data, $V_{cmax(25)}$ was estimated based on Sharkey et al. (2007) and Sharkey (2005). Note: the bars represent one standard deviation.

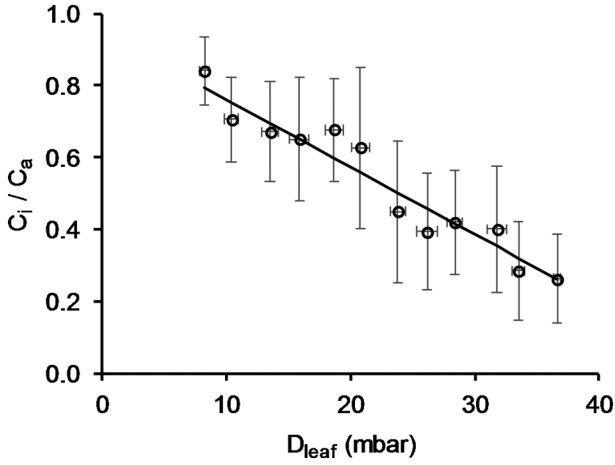

Figure 3 Decline in the ratio between intercellular CO_2 concentration (C_i) and ambient CO_2 concentration (C_a) with increasing leaf vapour pressure deficit (D_{leaf}) for 1- to 19-year-old oil palm trees (N = 654). Leaf gas exchanges were measured based on Long and Bernacchi (2003) using the TPS-2 Portable Photosynthesis System (PP Systems International, Inc., Amesbury, US). Note: the bars represent one standard deviation.

100.7 μmol CO_2 m^{-2} leaf s^{-1}, a value they had calculated based on the leaf N content and specific leaf area for crops in general (not specifically based on oil palm leaves).

The intercellular CO_2 concentration (C_i) can be determined from its relationship with ambient CO_2 concentration (C_a) (both concentrations expressed as μmol CO_2 mol^{-1} air) and vapour pressure deficit in the leaves by the following equation by Yin and van Laar (2005):

$$C_i / C_a = 1 - \left(1 - \Gamma^* / C_a\right)\left(a + bD_{leaf}\right) \tag{18}$$

where D_{leaf} is the leaf vapour pressure deficit (mbar), determined by

$$D_{leaf} = e_s\left[\!\left[T_f\right]\!\right] - e_a \tag{19}$$

where $e_s\left[\!\left[T_f\right]\!\right]$ is the saturated vapour pressure (mbar) at foliage temperature T_f (°C) and e_a is the air vapour pressure (mbar). Leaf measurements on of oil palm trees at various ages (from 1 to 19 years) revealed that coefficients *a* and *b* are 0.0615 and 0.0213, respectively (Fig. 3).

4.2 Light-limited assimilation (v_q)

Light-limited leaf CO_2 assimilation rate v_q is determined by

$$v_{q,sl/sh} = 0.8 e_m Q_{sl/sh}\left(C_i - \Gamma^*\right) / \left(C_i + \Gamma^*\right) \tag{20}$$

where $v_{q,sl/sh}$ is the light-limited leaf CO_2 assimilation rate (μmol CO_2 m^{-2} leaf s^{-1}) for either sunlit (subscript *sl*) or shaded (*sh*) leaves; $Q_{sl/sh}$ is the photosynthetically active radiation

(PAR) flux density absorbed by either sunlit or shaded leaves (μmol m^{-2} leaf s^{-1}); and e_m is the intrinsic quantum efficiency or yield (μmol CO_2 μmol^{-1} photons), taken as 0.051 for oil palm (Dufrêne and Saugier, 1993). Skillman (2008) reviewed 10 studies that measured e_m of various C3 plants and the mean value (± s.e.) was found to be 0.052 ± 0.003 (N = 61).

According to Campbell and Norman (1998), there are four PAR flux components within the canopies, namely: 1) PAR irradiance for unintercepted beam *with* scattering $Q_{p,dr}$ (μmol photons m^{-2} ground s^{-1}), 2) PAR irradiance for unintercepted beam *without* scattering $Q_{p,dr,dr}$ (μmol photons m^{-2} ground s^{-1}), 3) PAR irradiance of *only* the scattered component $Q_{p,dr,\alpha}$ (μmol photons m^{-2} leaf s^{-1}) and 4) mean diffuse PAR irradiance $\overline{Q_{p,df}}$ (μmol photons m^{-2} leaf s^{-1}). Note that both $Q_{p,dr,\alpha}$ and $\overline{Q_{p,df}}$ are expressed based on per unit leaf area (not per unit ground area). The scattered and diffuse irradiance on a unit horizontal ground area are assumed equal to their irradiance on a unit leaf area. These four PAR flux components can be calculated by

$$Q_{p,dr} = (1-p_{dr})Q_{dr}exp\left(-k_{dr}\omega\sqrt{0.8}L\right) \tag{21}$$

$$Q_{p,dr,dr} = (1-p_{dr})Q_{dr}exp\left(-k_{dr}\omega L\right) \tag{22}$$

$$Q_{p,dr,\alpha} = \left(Q_{p,dr} - Q_{p,dr,dr}\right)/2 \tag{23}$$

$$\overline{Q_{p,df}} = (1-p_{df})Q_{df}\left[1-exp\left(-k_{df}\sqrt{0.8}L\right)\right]/k_{df}L \tag{24}$$

where Q_{dr} and Q_{df} are the instantaneous direct and diffuse PAR irradiance, respectively (both in μmol photons m^{-2} ground s^{-1}); p_{dr} and p_{df} are the canopy reflection coefficients for direct and diffuse PAR, respectively (both unitless); k_{dr} and k_{df} are the canopy extinction coefficients for direct and diffuse PAR, respectively (both unitless); ω is the canopy clustering coefficient for discontinuous canopies (0 to 1); and L is the total leaf area index (m^2 leaf m^{-2} ground).

The PAR irradiance components Q_{dr} and Q_{df} are determined by

$$Q_{dr} = I_{dr} \times 4.55 \times 0.5 \tag{25}$$

$$Q_{df} = I_{df} \times 4.55 \times 0.5 \tag{26}$$

where I_{dr} and I_{df} are the instantaneous direct and diffuse solar irradiance, respectively (W m^{-2} ground). Total PAR irradiance is assumed to be 50% of total solar irradiance, and 1 W m^{-2} ground is taken as equal to 4.55 μmol photons m^{-2} ground s^{-1} (Goudriaan and van Laar, 1994).

The reflection coefficients p_{dr} and p_{df} are determined according to Goudriaan (1977) by

$$p_{dr} = MAX\left[0.04, p_s exp\left(-2k_{dr}\omega\sqrt{0.8}L\right)\right] \tag{27}$$

$$p_{df} = MAX\left[0.04, p_s exp\left(-2k_{df}\sqrt{0.8}L\right)\right] \tag{28}$$

where p_s is the soil reflection coefficient, taken as 0.15.

Assuming the oil palm canopies are randomly distributed in the aerial space, the canopy extinction coefficient for direct PAR k_{dr} is determined by

$$k_{dr} = 0.5 / cos\theta \tag{29}$$

where θ is the solar inclination (radians). Equation 29, however, is valid only for fully closed canopies. For discontinuous or partially closed canopies, k_{dr} must be multiplied by a clump factor ω, which ranges from 0 (no canopy) to 1 (fully closed canopies), and which can be determined according to Kustas and Norman (1999) as

$$\omega = \omega_0 + 6.6557(1-\omega_0)exp\left[exp(-\theta + 2.2103)\right] \tag{30a}$$

$$\omega_0 = \frac{1}{k_{dr}L} ln\left\{\tau_b + (1-\tau_b)exp\left[-k_{dr}\frac{L}{1-\tau_b}\right]\right\} \tag{30b}$$

where ω_0 is the canopy clustering coefficient when the sun is at zenith (highest point in the sky) and τ_b is the canopy gap fraction (0 to 1). Awal (2008) measured the canopy gap fraction for various oil palm tree ages, and reanalysing and fitting the best function to his measured data, τ_b can be estimated from L by

$$\tau_b = \left(1+1.33\sqrt{L}\right)^{-1} \tag{31}$$

Following the method by Teh (2006), the canopy extinction coefficient for diffuse PAR k_{df} is determined by integrating the light penetration function based on Beer's law (together with Eq. 29–31) over the whole sky (assuming a uniform bright sky) and for several leaf area indexes L to finally obtain the following estimate of k_{df}:

$$k_{df} = exp\left(0.038042 - 0.38845\sqrt{L}\right) \tag{32}$$

Note that this k_{df} estimation already accounts for discontinuous canopies by the use of Eq. 30 in the integration.

The PAR flux densities absorbed by the oil palm canopy are made up of two components: that absorbed by the canopy directly exposed to direct PAR (sunlit portion of L) and that absorbed by the portion of canopy shaded from direct PAR (shaded L). Dividing the oil palm canopies in this way, rather than treating the canopies as one whole, would provide a more accurate estimation of canopy photosynthesis because the CO_2 assimilation by the sunlit and shaded portions of the canopies would often be different from each other.

L_{sl} and L_{sh} are the sunlit and shaded leaf area indexes, respectively (both in m^2 leaf m^{-2} ground), and they can be estimated according to Goudriaan and van Laar (1994) as

$$L_{sl} = \frac{1-exp(-k_{dr}\omega L)}{k_{dr}\omega} \tag{33}$$

$$L_{sh} = L - L_{sl} \tag{34}$$

Q_{sl} and Q_{sh} are the PAR flux densities absorbed by the sunlit leaves and shaded leaves, respectively (both in μmol photons m^{-2} leaf s^{-1}), and they can be determined according to Campbell and Norman (1998) as

$$Q_{sl} = 0.8\left(k_{dr}\omega Q_{dr} + \overline{Q_{p,df}} + Q_{p,dr,\alpha}\right) \tag{35}$$

$$Q_{sh} = 0.8\left(\overline{Q_{p,df}} + Q_{p,dr,\alpha}\right)p1 \tag{36}$$

Note that the PAR flux densities absorbed (Q_{sl} and Q_{sh}) are on a per unit leaf area (not per unit ground area basis).

4.3 Sink-limited assimilation (v_s)

Besides limitations by Rubisco and light, photosynthesis could also be limited by the amount of sink in the oil palm, as the greater the storage or sink, the slower the photosynthetic rate, akin to chemical reactions which slow down due to the buildup of assimilates. In a plant, the most likely limiting sink is the storage of sucrose, and Collatz et al. (1991) assumed that v_s is merely half of the maximum Rubisco capacity rate:

$$v_s = 0.5V_{cmax} \tag{37}$$

5 Modelling energy balance

The energy balance of the soil–plant–atmosphere system is described as a network of resistances in which latent and sensible heat fluxes must traverse within the system to reach some reference level above the canopy (Fig. 4) (Shuttleworth and Wallace, 1985). Solving the energy balance equation gives the potential water loss by soil evaporation and plant transpiration.

The energy balance in Fig. 4 can be described in eight independent equations, and as shown by Teh (2006) and Shuttleworth and Wallace (1985), these equations can be solved and summarized by the following series of equations to determine the total latent heat flux:

$$\lambda ET = C_c PM_c + C_s PM_s \tag{38a}$$

$$PM_c = \frac{\Delta A + \left(\rho c_p D - \Delta r_a^c A_s\right)/\left(r_a^a + r_a^c\right)}{\Delta + \gamma\left[1 + r_s^c/\left(r_a^a + r_a^c\right)\right]} \tag{38b}$$

$$PM_s = \frac{\Delta A + \left(\rho c_p D - \Delta r_a^s A_c\right)/\left(r_a^a + r_a^s\right)}{\Delta + \gamma\left[1 + r_s^s/\left(r_a^a + r_a^s\right)\right]} \tag{38c}$$

$$C_c = \left\{1 + R_c R_a/\left[R_s\left(R_c + R_a\right)\right]\right\}^{-1} \tag{38d}$$

$$C_s = \left\{1 + R_s R_a/\left[R_c\left(R_s + R_a\right)\right]\right\}^{-1} \tag{38e}$$

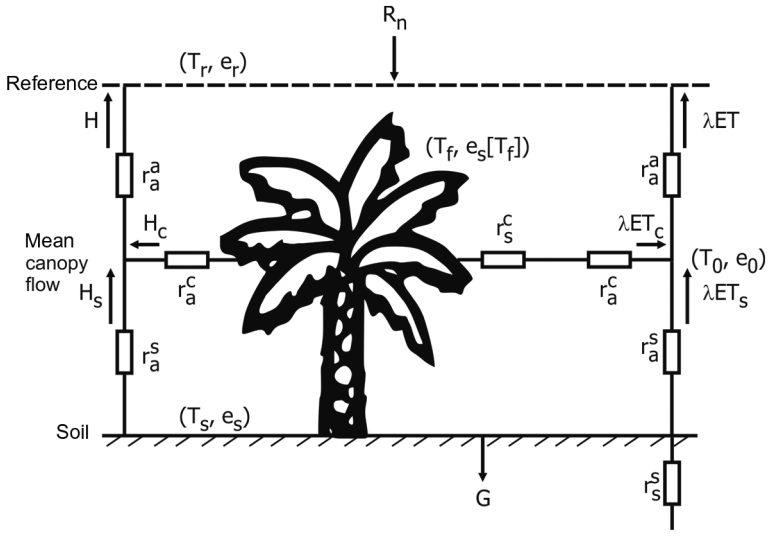

Figure 4 Energy balance of the oil palm system described as a network of resistances. Key: λET and H are components of the latent and sensible heat fluxes, respectively; R_n is the net radiation flux; G is the heat flux into the soil; T and e are the temperature and vapour pressure components; $e_s[\![T]\!]$ is the saturated vapour pressure at temperature T; r_a^a and r_a^s are the aerodynamic resistances; and r_a^c, r_s^c and r_s^s are the surface resistances.

$$R_a = (\Delta + \gamma) r_a^a \tag{38f}$$

$$R_c = (\Delta + \gamma) r_a^c + \gamma r_s^c \tag{38g}$$

$$R_s = (\Delta + \gamma) r_a^s + \gamma r_s^s \tag{38h}$$

where λET is the total latent heat flux (W m^{-2}); r_a^a is the aerodynamic resistance between the mean canopy flow and reference height (s m^{-1}); r_a^s is the aerodynamic resistance between the soil and mean canopy flow (s m^{-1}); r_a^c is the bulk boundary layer resistance (s m^{-1}); r_s^c and r_s^s are the canopy and soil surface resistance, respectively (both in s m^{-1}); A, A_s and A_c are energy available to the system (total), soil and crop, respectively (all in W m^{-2}); Δ is the slope of the saturated vapour pressure curve (mbar K^{-1}); γ is the psychometric constant (0.658 mbar K^{-1}); D is the air vapour pressure deficit (mbar) and ρc_p is the volumetric heat capacity for air (1221.09 J m^{-3} K^{-1}).

Determination of total latent heat flux λET allows the determination of the vapour pressure deficit D_0 (mbar) at the theoretical mean canopy flow height as

$$D_0 = D + \frac{r_a^a}{\rho c_p}\left[\Delta A - (\Delta + \gamma)\lambda ET\right] \tag{39}$$

so that D_0 can in turn be used to determine the partitioning of the total latent heat flux λET and total sensible heat flux H into their respective soil (λET_s and H_s) and crop (λET_c and H_c) flux components:

$$\lambda ET_s = \frac{\Delta A_s + \rho c_p D_0 / r_a^s}{\Delta + \gamma\left(r_s^s + r_a^s\right)/r_a^s} \tag{40}$$

$$\lambda ET_c = \frac{\Delta A_c + \rho c_p D_0 / r_a^c}{\Delta + \gamma\left(r_s^c + r_a^c\right)/r_a^c} \tag{41}$$

$$H_s = \frac{\gamma A_s\left(r_s^s + r_a^s\right) - \rho c_p D_0}{\Delta r_a^s + \gamma\left(r_s^s + r_a^s\right)} \tag{42}$$

$$H_c = \frac{\gamma A_c\left(r_s^c + r_a^c\right) - \rho c_p D_0}{\Delta r_a^c + \gamma\left(r_s^c + r_a^c\right)} \tag{43}$$

where all the soil and crop flux components are in W m^{-2}.

Numerical Gaussian integration method is used to obtain the daily latent heat and sensible fluxes (Teh, 2006). The daily amount of water transpired (by plants) and evaporated (by soil) are estimated by such integration methods. Five points over 24 hours in a day were selected, and for each selected hour, the heat fluxes were calculated.

5.1 Available energy

The balance of net radiation R_n after subtracting soil heat flux G is the energy available to the plant A_c and soil A_s (all in W m^{-2}), or

$$A = A_s + A_c = R_n - G \tag{44a}$$

$$A_s = R_n \tau_{dr,\alpha} - G \tag{44b}$$

$$A_c = R_n\left(1 - \tau_{dr,\alpha}\right) \tag{44c}$$

$$G = R_n\left[t_c + \tau_{dr,\alpha}\left(t_s - t_c\right)\right] \tag{44d}$$

$$\tau_{dr,\alpha} = exp\left(-k_{dr}\omega\sqrt{0.5}L\right) \tag{44e}$$

where L is the total leaf area index (m^2 leaf m^{-2} ground); k_{dr} is the canopy extinction coefficient for direct solar radiation; ω is the canopy clustering coefficient; and t_c and t_s are the fraction of net radiation available as soil heat flux under full canopies and for bare soil (no canopies), respectively. Parameters t_c and t_s are taken as 0.05 (Monteith, 1973) and 0.315 (Kustas and Daughtry, 1990), respectively.

Following Brutsaert (1982), net radiation R_n (W m^{-2}) is determined as the difference between the incoming shortwave radiation I_t (W m^{-2}) and outgoing net long-wave radiation R_{nL} (W m^{-2}):

$$R_n = (1-p)I_t + R_{nL} \tag{45a}$$

$$R_{nL} = 0.98\sigma(T_a + 273.15)^4\left[1.31\left(\frac{e_a}{T_a + 273.15}\right)^{1/7} - 1\right] \tag{45b}$$

where p is the surface albedo (0.15) and σ is the Stefan-Boltzmann constant (5.67 × 10^{-8} W m^{-2} K^{-4}).

5.2 Vertical profile of wind speed and eddy diffusivity

Wind speed decreases exponentially with decreasing height due to increasing drag until wind speed theoretically reaches zero at a height equal to the total height of zero plane displacement d and crop roughness length z_0. The methods by Su et al. (2001) and Massman (1997) were adapted to determine d and z_0 (both in m) as

$$d = h\Delta H \tag{46a}$$

$$z_0 = h(1-\Delta H)exp(-k/0.32) \tag{46b}$$

$$\Delta H = 1 - \frac{exp(-2k_w)\left[exp(-2k_w)-1\right]}{2k_w} \quad \text{for } 0.30 \le \Delta H \le 0.95 \tag{46c}$$

where k_w is the vertical wind speed extinction coefficient (unitless); h is the tree height (m) and k is the von Karman constant (0.4).

Vertical wind speed extinction coefficient k_w (assumed equal to eddy diffusivity k_e) increases with increasing leaf area index. Simulations by Massman (1987) for hypothetical canopies with uniform foliage density were used by Nikolov and Zeller (2003) to approximate the relationship between k_w and total leaf area index L (m^2 leaf m^{-2} ground) simply as

$$k_w = k_e = 3\left[1-\exp(-L)\right] \tag{47}$$

The wind speed at the canopy height u_h (m s^{-1}) is determined by

$$u_h = \frac{u_*}{k} ln\left(\frac{h-d}{z_0}\right) \tag{48}$$

where u_* is the friction velocity (m s^{-1}), determined by

$$u_* = \frac{ku}{ln\left(\frac{z_r - d}{z_0}\right)} \tag{49}$$

where u is the wind speed (m s^{-1}) measured at the reference height z_r (m).

5.3 Resistances

Aerodynamic resistances are calculated by

$$r_a^s = \frac{exp(k_e)}{k_e k u_*}\left[exp\left(-k_e \frac{z_{s0}}{h}\right) - exp\left(-k_e \frac{z_0 + d}{h}\right)\right] \quad (50)$$

$$r_a^a = \frac{1}{k_e u_*} ln\left(\frac{z_r - d}{h - d}\right) + \frac{1}{k_e k u_*}\left\{exp\left[k_e\left(1 - \frac{z_0 + d}{h}\right)\right] - 1\right\} \quad (51)$$

where r_a^s and r_a^a are the aerodynamic resistance between the mean canopy flow and reference height and between the soil and mean canopy flow, respectively (both in s m^{-1}); and z_{s0} is the soil surface roughness length (m), taken as 0.004, the value for a flat, tilled land (Hansen, 1993).

Calculations are adapted from Campbell and Norman (1998) to determine the bulk boundary layer resistance r_a^c (s m^{-1}) as

$$r_a^c = \frac{k_w}{0.01 L_{eff}\left[1 - exp(-0.5 k_w)\right]\sqrt{u_h / w}} \quad (52)$$

where L_{eff} is the effective leaf area index (m^2 leaf m^{-2} ground); and w is the mean leaf width (m), which, for oil palm pinnae, can be determined from the work by Rao et al. (1992) as

$$w = 0.0165 + 0.0152 ln(age / 365) \quad (53)$$

where *age* refers to the tree age (days).

Not all leaves, especially at near or full canopy, would contribute equally to affect fluxes. This is due to self-shading of leaves. Consequently, Szeicz and Long (1969) recommended that an effective leaf area index L_{eff} be used instead of total L, where L_{eff} is taken as the smaller value of the the current leaf area index L and half of the maximum possible leaf area index; that is,

$$L_{eff} = MIN[L,\ 0.5 L_{max,PD}] \quad (54)$$

where $L_{max,PD}$ is the maximum leaf area index (m^2 leaf m^{-2} ground) for a given PD planting density (palms ha^{-1}), and for oil palm, $L_{max,PD}$ is determined by

$$L_{max,PD} = 0.0274 PD^{1/A} \quad (55)$$

where A is 0.935. Equation 55 was derived by fitting the best function to the maximum L obtained in various oil palm planting densities from Foong (1999), Kwan (1994), Rao et al. (1992) and Tan and Ng (1977).

Canopy resistance is determined by scaling up leaf stomatal resistance (the inverse of leaf stomatal conductance) to the canopy level by

$$r_s^c = 1 / (gst \times L_{eff}) \quad (56)$$

where r_s^c is the canopy resistance (s m^{-1}) and gst is the leaf stomatal conductance (m s^{-1}).

Leaf stomatal conductance gst is at maximum conductance gst_{max}, but water stress, low PAR irradiance, and vapour pressure deficit will reduce gst by the following relationships:

$$gst = gst_{max} \times f_{water} \times f_{PAR} \times f_D \quad (57a)$$

$$f_{water} = ET_c / PET_c \tag{57b}$$

$$f_{PAR} = gst_{PAR}[\![PAR]\!] / gst_{PAR}[\![PAR_{max}]\!] \tag{57c}$$

$$gst_{PAR}[\![PAR]\!] = 0.014614\left[1 - exp\left(-0.008740PAR\right)\right] \tag{57d}$$

$$f_D = gst_D[\![D]\!] / gst_D[\![D_{min}]\!] \tag{57e}$$

$$gst_D[\![D]\!] = 0.031970 - 0.007516ln(D) \tag{57f}$$

where gst_{max} for oil palm is 500 mmol H_2O m^{-2} leaf s^{-1} or 0.0125 m s^{-1} (Kallarackal et al., 2004); and f_{PAR}, f_{water} and f_D are scaled reductions from 0 to 1 to gst_{max} due to PAR irradiance, water stress and vapour pressure deficit, respectively.

Note that crop water stress is described in Eq. 57b, where the level of stress is determined, following Kropff (1993), as the ratio of the actual to potential transpiration (ET_c and PET_c, respectively; both in m day^{-1}).

Equations 57d and 57f were derived by fitting the best functions to measured leaf stomatal conductance at several levels of PAR and air vapour pressure deficit *D* (Fig. 5). Leaf stomatal conductance for palm aged 1–20 years was measured using the AP4 dynamic diffusion porometer (Delta-T Devices Ltd., Cambridge, UK). From Fig. 5a, PAR_{max}, which is the maximum PAR irradiance (W m^{-2}) for maximum leaf conductance, is taken at 330 W m^{-2} (or 1500 µmol photons m^{-2} ground s^{-1}) (Dufrêne and Saugier, 1993). Similarly, maximum conductance occurs when air vapour pressure deficit is minimum (D_{min}), taken at 10 mbar (Fig. 5b).

Finally, soil surface resistance r_s^s (s m^{-1}) was determined solely from the first (topmost) soil layer as this is the layer in direct contact with the atmosphere. Equations from Farahani and Ahuja (1996) and Choudhury and Monteith (1988) are used:

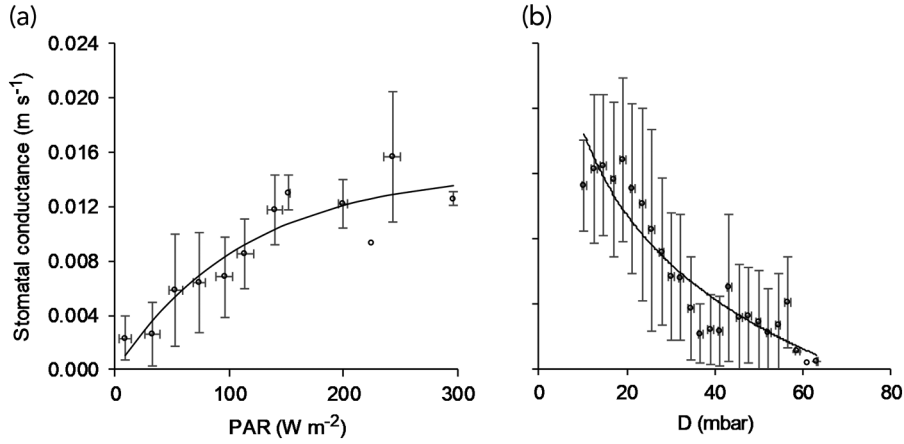

Figure 5 Relationship between measured leaf stomatal conductance with: (a) photosynthetically active radiation (PAR) irradiance (N = 381) and (b) air vapour pressure deficit *D* (N = 2591). Leaf measurements were made on 1- to 20-year-old oil palm trees. Note: the bars represent one standard deviation.

$$r_s^s = \frac{\tau l}{\phi_p D_{m,v}} exp\left(-\frac{1}{\lambda} \times \frac{\theta}{\theta_0}\right) \tag{58}$$

where $D_{m,v}$ is the vapour diffusion coefficient in air (24.7×10^{-6} m^2 s^{-1}); ϕ_p is the soil porosity (m^3 m^{-3}); l is the soil layer thickness of the first soil layer (m); θ is the volumetric soil water content (m^3 m^{-3}); θ_0 is the saturated soil water content (m^3 m^{-3}); λ is the soil pore-size distribution index or the slope of the logarithmic suction–soil moisture curve (Bittelli et al. 2015) and τ is the soil tortuosity (unitless), determined from Shen and Chen (2007) as

$$\tau = \sqrt{\phi_p + 3.79\left(1-\phi_p\right)}, \tag{59}$$

Soil properties and water flow in oil palm plantations are discussed next.

6 Modelling soil water flow

Rather than treating the whole soil profile as one large and homogeneous soil layer, it is more accurate to divide the soil profile into two or more soil layers and then use Darcy's law to describe the flow of water from one soil layer to the next, taking into account the physical properties of each soil layer (Fig. 6). Water flow is modelled following the 'tipping bucket' system, where water flow is treated in a sequential manner, beginning in the first soil layer, then moving successively down through the soil profile until the last soil layer (Hillel, 1977).

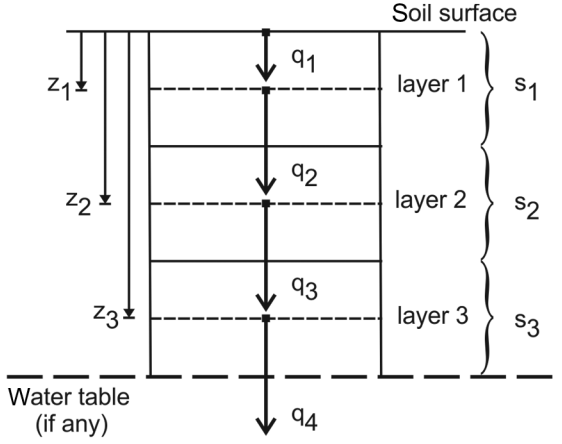

s_i = thickness of soil layer *i* (m)
z_i = depth of the middle of soil layer *i* from the surface (m)
q_i = water flux into soil layer *i* (m day^{-1})

Figure 6 Water flow in a soil profile is divided into three successive layers, with the presence of a water table, if any, always just beneath the last (in this case, third) soil layer.

It is recommended to divide a soil profile into two or more consecutive layers, with the first soil layer as a thin layer and the second layer covering up to at least the entire rooting depth. Soil layer i (i = 1 to N) has a thickness of s_i (m), and the depth from the soil surface to the middle of layer i is z_i.

Water flux into soil layer i is denoted as q_i (m day^{-1}). Water flow follows the downward positive coordinate system, where the downward and upward directions of flow of water are taken as a positive and negative value, respectively, and the reference level is taken as the soil surface level. Darcy's law is used to describe the water flow in the soil. Water flow is taken to occur from the middle of layer $i-1$ to the middle of layer i. The method based on Hillel (1977) is followed. Water flux into soil layer i is:

$$q_i = \begin{cases} P_{net} - ET_s - ET_{c,i} & i = 1 \\ \overline{K_{\theta,i}} \dfrac{H_i - H_{i-1}}{z_i - z_{i-1}} - ET_{c,i} & 1 < i \le N \\ K_{\theta,N} & i = N+1 \end{cases} \tag{60a}$$

$$\overline{K_{\theta,i}} = \frac{K_{\theta,i-1} - K_{\theta,i}}{lnK_{\theta,i-1} - lnK_{\theta,i}} \tag{60b}$$

where q is the water flux (m day^{-1}); P_{net} is the net daily rainfall (m day^{-1}); ET_s is the actual daily soil evaporation (which occurs only from the first soil layer) (m day^{-1}); ET_c is the daily extraction of water by roots (actual plant transpiration) (m day^{-1}); $\overline{K_{\theta,i}}$ is the logarithmic mean of the hydraulic conductivities of layer i and $i-1$ (m day^{-1}); z is the soil layer's depth (m) and H is the total head (matric suction and gravity heads) (m). Note that water table, if present, is treated as an additional but saturated soil layer N+1, and Eq. 60 is used to describe the capillary rise of water.

Water flux out of the last soil layer ($i = N$) is denoted by q_{N+1}, and without the presence of a water table, it is merely equal to $K_{\theta,N}$ because it is assumed that the soil below the last layer is uniformly wet and that it has the same water content as the last soil layer. Consequently, water flux is only due to gravity gradient (no matric suction gradient). In this case, $q_{N+1} = K_{\theta,N}$.

The net flux $\widehat{q_i}$ (m day^{-1}) in soil layer i is the difference between incoming q_i and outgoing water q_{i+1} fluxes:

$$\widehat{q_i} = q_{i-1} - q_{i+1} \tag{61}$$

where a positive net flux means soil water content has increased, and in contrast, a negative net flux denotes the soil is drying. This means that the change in the soil water content is determined by:

$$\Theta_{i,t+1} = \Theta_{i,t} + \widehat{q_i} \tag{62}$$

where $\Theta_{i,t}$ and $\Theta_{i,t+1}$ are the water content in soil layer i (m) between two successive time steps t and t+1, respectively.

For each soil layer i, the volumetric soil water content (m^3 m^{-3}) at permanent wilting point θ_{1500}, field capacity θ_{33} and saturation θ_0 are estimated from the soil's primary particles (clay and sand) and organic matter contents based on empirical equations from Saxton and Rawls (2006). Matric suction head and soil hydraulic conductivity (m day^{-1}) for saturated $K_{s,i}$ and unsaturated $K_{\theta,i}$ flows are estimated based on Bittelli et al. (2015) and Saxton and Rawls (2006), using the geometric mean distribution of the soil's primary particles.

Actual soil evaporation ET_s (taken as m day^{-1}) is calculated from Teh (2006) and van Keulen and Seligman (1987) as

$$ET_s = PET_s \times R_{Ds} \tag{63a}$$

$$R_{Ds} = \frac{1}{1+\left(3.607\theta_1 / \theta_{s,1}\right)^{-9.3172}} \tag{63b}$$

where PET_s is the potential evaporation (m day^{-1}); R_{Ds} is the reduction factor for evaporation (ranging from 0 to 1); and θ_1 and $\theta_{s,1}$ are the current and saturated soil water content, respectively, for the first soil layer (i = 1) (both in m^3 m^{-3}). Note: λET_s (W m^{-2}) from Eq. 40 is divided by λ (2454000 J kg^{-1}) and multiplied by 86.4 to obtain PET_s in m day^{-1}.

Actual transpiration (ET_c, m day^{-1}) is calculated from Kropff (1993) as

$$ET_c = PET_c \times R_{Dc} \tag{64a}$$

$$R_{Dc} = \begin{cases} 1 & \theta_{root} \geq \theta_{cr,root} \\ \dfrac{\theta_{root} - \theta_{1500,root}}{\theta_{cr,root} - \theta_{1500,root}} & \theta_{1500,root} < \theta_{root} < \theta_{cr,root} \\ 0 & \theta_{root} \leq \theta_{1500,root} \end{cases} \tag{64b}$$

$$\theta_{cr,root} = \theta_{1500,root} + p\left(\theta_{0,root} - \theta_{1500,root}\right) \tag{64c}$$

where PET_c is the potential transpiration (after converting λET_c from Eq. 41 into m day^{-1}); R_{Dc} is the reduction factor for transpiration (0 to 1); θ_{root} is the soil water content currently in the root zone; $\theta_{1500,root}$ and $\theta_{0,root}$ are the soil root zone's permanent wilting and saturation points, respectively; and $\theta_{cr,root}$ is the volumetric water content in the root zone below which water stress occurs. All soil water contents are expressed in m^3 m^{-3}.

For C3 plants in general, p in Eq. 64c is often taken as 0.5. However, a comparison of the soil water content between irrigated and non-irrigated oil palm trials from 1983 to 1990 by Foong (1999) suggested that oil palm is more sensitive to water stress because p is more likely 0.6 than 0.5 of $\left(\theta_{0,root} - \theta_{1500,root}\right)$. This 0.6 critical point corresponds to about 45% of the available soil water content (AWC) of Munchong soil series (Typic Hapludox), the type of soil in the oil palm trials by Foong (1999). Incidentally, Rey et al. (1998) also observed that oil palm stomatal conductance would begin to decline only when the soil water content fell below the level of about 50% of their soil's AWC (Fig. 7).

The amount of water extracted by roots in each soil layer is based on the measured data for oil palm by Nelson et al. (2006) and on the root water uptake algorithm by Miyazaki (2005):

$$ET_{c,i} = ET_c\left(\varphi_i - \varphi_{i-1}\right) \tag{65a}$$

$$\varphi_i = 1.8c_j - 0.8c_j^2 \tag{65b}$$

$$c_j = MIN\left[1,\ S_j / d_{root}\right] \tag{65c}$$

where S_j is the cumulative thickness of soil layer j (summation of thickness of the current soil layer and all its preceding soil layers).

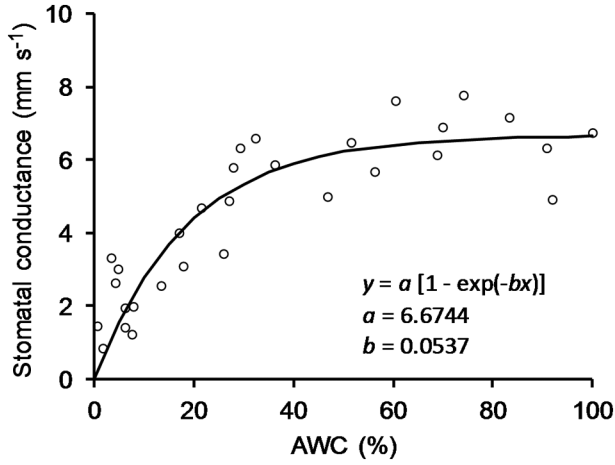

Figure 7 Fitting the best function to the relationship between oil palm leaf stomatal conductance and available soil water content (AWC), as measured by Rey et al. (1998). Stomatal conductance declined only when AWC was about 50% or less.

Lastly, net rainfall P_{net} refers to the amount of rain reaching the ground as both throughfall and stemflow. The larger the canopy cover or leaf area index, the larger the fraction of intercepted gross rainfall by the canopies and the smaller the net rainfall. Net rainfall studies on closed oil palm canopies by Lubis (2016), Chong (2012), Bentley (2007), Zulkifli et al. (2006) and Damih (1995) showed that throughfall and stemflow account for on average (± s.e.) 61.3 ± 2.1 and 8.4 ± 1.0% of P_g, respectively (N = 430 rain events). P_{net} (m day^{-1}) is related to oil palm leaf area index L (m^2 leaf m^{-2} ground) and P_g (m day^1) as follows:

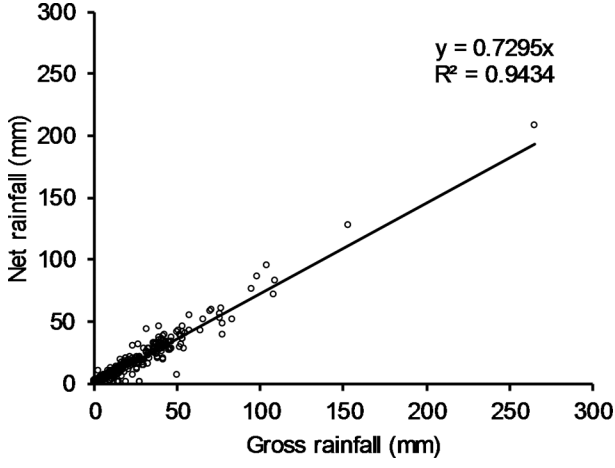

Figure 8 Strong linear relationship between net rainfall and gross rainfall under closed oil palm canopies (Lubis 2016; Chong 2012; Bentley, 2007; Zulkifli et al. 2006; Damih 1995) (N = 430).

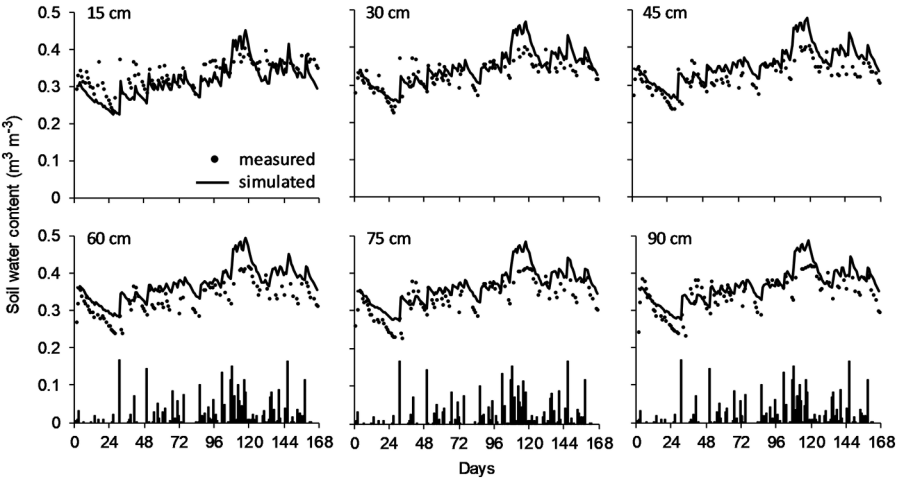

Figure 9 Comparisons between simulated and measured soil water content at several soil depths (from 15 to 90 cm) under fully matured oil palms. Note: the bar charts in the lower panel represent the daily rainfall amount (mm) (total rainfall during this period was 1890 mm, with a maximum daily rainfall of 100 mm).

$$P_{net} = P_g \times MAX[\![0.7295,\ 1-0.0541L]\!] \tag{66}$$

where it is assumed that P_{net} / P_g decreases linearly with L until closed canopies are reached, after which P_{net} never exceeds 72.95% of P_g (Fig. 8). Figure 9 shows the accuracy of this soil water model component when it was tested against field measurements of soil water content at several soil depths (0.15–0.90 m) under fully matured oil palms (20 years old; 148 palms ha 1) in an oil palm estate at Serdang, Malaysia (2.98053403°N, 101.72884214°E). Daily soil water measurements were made for 167 days from 17 July 2012. The soil type was Munchong series (Typic Hapludox), with a rather homogeneous soil profile (54% clay and 37% sand). The average absolute difference between soil water predictions and measurements was 0.03 $m^3\ m^{-3}$.

7 Modelling crop growth

Plant assimilates (expressed as amount of CH_2O) produced via photosynthesis are first used for plant maintenance respiration (supporting processes for continual plant survival) and vegetative growth respiration (synthesis of new cells) (Thornley 1970), after which the balance is then used for generative growth (development of flowers, bunches and yield). The method by van Kraalingen et al. (1989) for oil palm was adapted.

7.1 Maintenance respiration

The maintenance respiration for pinnae M_{pinnae}, rachis M_{rachis}, trunk M_{trunk} and roots M_{roots} (all in kg CH_2O $palm^{-1}$ day^{-1}) was calculated as follows:

$$M_{pinnae} = W_{pinnae} \times M_{c,pinnae} \times (24 - DL) / 24 \tag{67a}$$

$$M_{c,pinnae} = (N_{pinnae} \times 0.036 \times 6.25) + (X_{pinnae} \times 0.072 \times X_c) \quad (67b)$$

$$M_{rachis} = W_{pinnae} \times M_{c,rachis} \quad (68a)$$

$$M_{c,rachis} = (N_{rachis} \times 0.036 \times 6.25) + (X_{rachis} \times 0.072 \times X_c) \quad (68b)$$

$$M_{trunk} = (W_{top.trunk} + 0.06W_{bottom,trunk}) \times M_{c,trunk} \quad (69a)$$

$$M_{c,trunk} = (N_{trunk} \times 0.036 \times 6.25) + (X_{trunk} \times 0.072 \times X_c) \quad (69b)$$

$$W_{top,trunk} = MIN[W_{trunk}, 45.0]$$

$$W_{bottom,trunk} = W_{trunk} - W_{top,trunk} \quad (69c)$$

$$M_{roots} = W_{roots} \times M_{c,roots} \quad (70a)$$

$$M_{c,rachis} = (N_{roots} \times 0.036 \times 6.25) + (X_{roots} \times 0.072 \times X_c) \quad (70b)$$

where $W_{(part)}$ represents the dry weight (DM) of an individual plant part (*e.g.*, pinnae, rachis, trunk, or roots) (kg DM palm^{-1}); *DL* is the day length (hour) $M_{c,(part)}$ is the maintenance coefficient for each specific plant part (kg CH_2O kg^{-1} DM); $N_{(part)}$ and $X_{(part)}$ are the nitrogen and mineral fractions (by weight) in a given plant part, respectively; and X_c is the correction factor for mineral content (unitless), taken as 2 by van Kraalingen et al. (1989).

Maintenance respiration to generate new organs (bunches and flowers) M_{organs} (kg CH_2O kg^1 DM) is determined as follows:

$$M_{organs} = 0.0027W_{matbunch} + M_{c,rachis}\left(W_{immbunch} + W_{maleflo}\right) \quad (71)$$

where $W_{matbunch}$, $W_{immbunch}$ and $W_{maleflo}$ are the dry weights of the mature bunches, immature bunches and male flowers, respectively (kg DM palm^{-1}), and it is assumed that the maintenance coefficients for immature bunches and male flowers are the same as that for rachis.

Total maintenance is determined by:

$$M_{total} = M_{metabolic} + \sum\nolimits_{plant\ parts} M_{(part)} \quad (72a)$$

$$M_{metabolic} = \frac{0.16\Lambda_{canopy,d}}{\sum\nolimits_{plant\ parts} W_{(part)}} \quad (72b)$$

where M_{total} is the total maintenance requirement for the whole tree, which is the summation of the maintenance requirement for all plant parts, as well as that to support the metabolic activity $M_{metabolic}$ (all units in kg CH_2O palm^{-1} day^{-1}); $\Lambda_{canopy,d}$ is the daily canopy photosynthesis (Eq. 12) (kg CH_2O palm^{-1} day^{-1}) and $\sum_{plant\ parts} W_{(part)}$ is the total dry weight of all plant parts (kg DM palm^{-1}).

Maintenance respiration increases with increasing air temperature, so M_{total} must be corrected for air temperature. Correction was performed using Eq. 15 and taking the Q_{10} coefficient as 2. Growth of oil palm is completely inhibited when air temperature is below

15°C (Henry, 1955). The maximum air temperature for oil palm growth is taken as 45°C, a general maximum value for most plants (Hasanuzzaman et al., 2013). Consequently, if the current air temperature is beyond oil palm's growing temperature range of 15–45°C, all assimilates if any will solely be for maintenance respiration.

Any balance of assimilates after maintenance respiration is available for vegetative growth respiration G_{growth} (kg CH_2O palm^{-1} day^{-1}) as:

$$G_{growth} = MAX\left[0,\ \Lambda_{canopy,d} - M_{total}\right] \tag{73}$$

7.2 Vegetative growth respiration

The annual vegetative dry matter requirement *VDM* (kg DM palm^{-1} year^{-1}) is determined based on leaf area index *L* (m^2 leaf m^{-2} ground), following a rectangular hyperbola relationship, as

$$VDM = MIN\left[20,\ \left(a + b / L^{1.5}\right)^{-1}\right] \tag{74a}$$

$$a = A / VDM_{max,PD} \tag{74b}$$

$$b = 0.1(1/A - 1)(PD/100)^{1/A} \tag{74c}$$

$$VDM_{max,PD} = 231 PD^{1-1/A} \tag{74d}$$

where $VDM_{max,PD}$ is the maximum VDM for the given planting density *PD* (palms ha^{-1}) and *A* is 0.935. Coefficients *a*, *b* and *A*, as well as $VDM_{max,PD}$, were obtained by fitting the best functions to measured data from van Kraalingen et al. (1989).

The growth rates $G_{growth,(part)}$ (kg DM palm^{-1} day^{-1}) for the individual plant parts (pinnae, rachis, trunk and roots) are determined by

$$G_{growth,\ (part)} = DM_{(part)} \times A_{growth} \times CVF \tag{75a}$$

$$A_{growth} = MIN\left[\frac{VDM/365}{CVF},\ G_{growth}\right] \tag{75b}$$

$$CVF = 0.70\left(DM_{pinnae} + DM_{rachis}\right) + 0.66 DM_{trunk} + 0.65 DM_{roots} \tag{75c}$$

where A_{growth} is the actual amount of assimilates available for vegetative growth respiration (kg CH_2O palm^{-1} day^{-1}); *CVF* is a factor (kg DM kg^{-1} CH_2O) to convert a weight expressed on a CH_2O per weight basis to that on per dry matter (DM) basis. Dry matter partitioning $DM_{(part)}$ for pinnae, rachis, trunk and roots are 0.24, 0.46, 0.14 and 0.16, respectively (their mean values are from Henson and Mohd Tayeb 2003; Henson 1995; Corley et al. 1971). Dry matter partitioning would likely be affected by planting densities, nutritional status and water stress, but during model development, PySawit's simulations showed better fit with training data sets when constant dry matter partitioning was used instead.

The death rates (kg DM palm^{-1} day^{-1}) for leaves (pinnae and rachis) and roots are calculated according to Dr. Ian E. Henson (then at Malaysian Palm Oil Board; personal communication) as

$$G_{death,leaves} = 0.0016 W_{leaves} \begin{cases} 0 & age \leq 600 \\ \dfrac{age - 600}{2500 - 600} & 600 < age \leq 2500 \\ 1 & age > 2500 \end{cases} \quad (76)$$

$$G_{death,roots} = \frac{W_{roots}}{365} \times \begin{cases} 0 & age \leq 1200 \\ 0.0000959210^{-5} age - 0.115 & 1200 < age \leq 3285 \\ 0.2 & age > 3285 \end{cases} \quad (77)$$

where *age* refers to the tree age (days), and W_{leaves} and W_{roots} are the dry weights of leaves and roots, respectively (both in kg DM palm^{-1}).

The net increase in dry weight of a plant part is the difference between its growth and death rates between two successive time steps *t* and *t*+1:

$$W_{(part),t+1} = W_{(part),t} + G_{growth,(part)} - G_{death,(part)} \quad (78)$$

where $W_{(part)}$ is the dry weight of a given plant part (kg DM palm^{-1}). Note that there is no death rate for trunk: $G_{death,trunk} = 0$.

Leaf area index *L* (m^2 leaf m^{-2} ground) is determined from planting density *PD* and the pinnae's dry weight W_{pinnae} and specific leaf area *SLA* (m^2 leaf kg^{-1} DM):

$$L = W_{pinnae} \times SLA \times PD / 10000 \quad (79)$$

Any balance of assimilates after vegetative growth respiration is available for generative growth G_{gen} (kg CH_2O palm^{-1} day^{-1}) as:

$$G_{gen} = MAX\left[0,\ G_{growth} - A_{growth}\right] \quad (80)$$

7.3 Generative organ growth

The so-called 'boxcar train' technique described by van Kraalingen et al. (1989) was used to track the growth progress of generative organs, namely the male flowers, immature bunches (female flowers) and mature bunches (Fig. 10). Each train (one for each generative organ) comprises several boxcars whereby each boxcar represents an age class. The life-span of both male flowers and immature bunches are taken as 210 days (beginning from the time when sex spikelet is first visible), and 150 days before harvest for the mature bunches (Corley et al. 1995). Consequently, the boxcar train for male flowers and immature bunches consist of 210 one-day age classes and for mature bunches 150 one-day age classes.

The algorithm of this boxcar train technique essentially consists of two steps: 1) the weight of a generative organ is shifted to successively older age classes and 2) the weight is incremented according to the calculated growth rate. The lifespan of male flowers is set at 210 days, after which they will die. For the immature bunches, however, the day after 210 days marks the point of pollination, after which the growth of the pollinated bunch (i.e., mature bunch) will occur. To determine the growth rates of the generative organs, the following general equations are used:

$$G_{gen,(part)} = \left(f_{e,(part)} \times G_{gen} \times CVF_2\right) / n_{(part)} \tag{81a}$$

$$CVF_2 = 0.70\left(f_{e,maleflo} + f_{e,immbunch}\right) + 0.44 f_{e,matbunch} \tag{81b}$$

where $G_{gen,(part)}$ is the growth rate for a given generative organ (male flowers, immature bunches and mature bunches) (kg DM day^{-1}); G_{gen} is the total amount of assimilates available for generative growth (kg DM day^{-1}); CVF_2 is a factor (kg DM kg^{-1} CH_2O) to convert dry matter weight into CH_2O weight; $n_{(part)}$ is the number (count) of a given generative organ currently maintained; and $f_{e,immbunch}$, $f_{e,matbunch}$ and $f_{e,maleflo}$ are the scaled fraction of dry matter to immature bunches, mature bunches and male flowers, respectively (all in fraction), where they are determined by

$$f_{e,(part)} = \frac{f_{(part)}}{\sum_{generative\ organs} f_{(part)}} \tag{82a}$$

$$f_{(part)} = DM_{(part)} \times n_{(part)} / N_{(part)} \tag{82b}$$

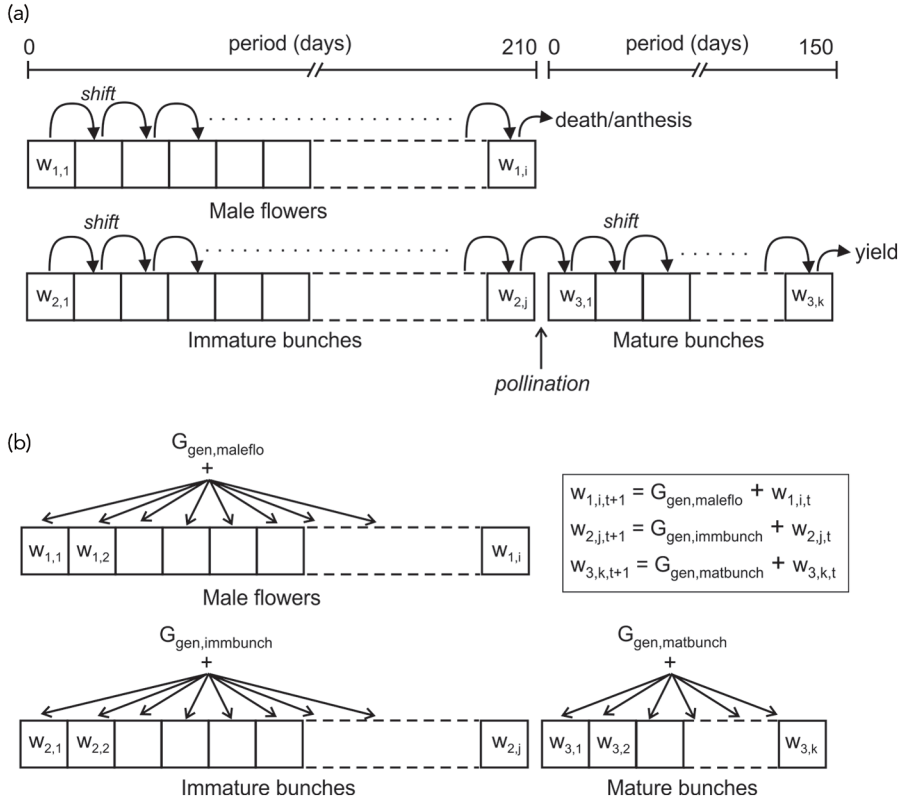

Figure 10 Boxcar train scheme for growth of generative organs. In every model time step, (a) weights are shifted to next age class, then (b) they are incremented by the growth rate of the generative organs.

where for a given generative organ, $DM_{(part)}$ is its share of assimilates available for generative growth (fraction) and $N_{(part)}$ is its total growth (maturity) length (210 days for male flowers and immature bunches and 150 days for mature bunches; Fig. 10). $DM_{(part)}$ for male flowers, immature bunches and mature bunches are 0.159, 0.159 and 0.682, respectively.

In the original model from van Kraalingen et al. (1989), both male and female flowers occur in equal proportions (50:50%) and without any flower abortion. PySawit model introduces an algorithm for flower sex determination whereby if a generated random value is smaller than or equal to a preset female probability p_{female}, then the new flower is female, else male:

$$sex\ of\ new\ flower = \begin{cases} female & r \le p_{female} \\ male & r > p_{female} \end{cases} \tag{83}$$

where p_{female} is the probability of having female flowers (0 to 1; 0 = no chance of female and 1 = always female) and r is a random variable uniformly distributed on [0 to 1). If p_{female} = 0.5, the tendency is to have equal proportions of male and female flowers. Consequently, the p_{female} parameter can be regarded as the genetic tendency of an oil palm planting material to produce female flowers.

Flower abortion occurs at 9 months before harvest (Corley et al. 1995), and abortion occurs if a generated random value is larger than the crop water stress level R_{Dc} (from Eq. 64b):

$$flower\ aborted? = \begin{cases} no & r \le R_{Dc} \\ yes & r > R_{Dc} \end{cases} \tag{84}$$

Consequently, the higher the level of water stress, the smaller the value of R_{Dc} and the greater the risk of flower abortion.

The generative organ weights are incremented between two successive time steps t and t+1 simply by

$$w_{(part),i,t+1} = \begin{cases} 0 & w_{(part),i,t} = 0 \\ w_{(part),i,t} + G_{gen,(part)} & w_{(part),i,t} > 0 \end{cases} \tag{85}$$

where $w_{(part),i}$ is the dry weight of a given generative organ in age class i (kg DM). The organ weights are incremented only for non-zero current weights. Thus, the total weight for a given generative organ is the summation of weights in all the age classes:

$$W_{(part)} = \sum_{i=1}^{N_{(part)}} w_{(part),i} \tag{86}$$

where $N_{(part)}$ is the total maturity period for a given generative organ (days).

7.4 Tree height and rooting depth

Measured oil palm trunk height data from Henson and Mohd Tayeb (2003), Kwan (1994), Rao et al. (1992), Breure and Powell (1988) and Jacquemard (1979, 1998) were used to develop the following equations to determine the initial trunk height $h_{trunk(initial)}$ (m) and rate of trunk height growth h'_{trunk} (m day^{-1}). Both are functions of tree age (days) and planting density PD (palms ha^{-1}):

$$h_{trunk(initial)} = \exp\left(2.846 - 1980.888 / PD^2 - 5166.366 / age\right) \quad (87)$$

$$h'_{trunk} = \frac{5166.366 h_{trunk(initial)}}{age^2} \times \frac{(0.210 R_{Dc} + 0.553)}{0.7} \quad (88)$$

where R_{Dc} is the crop water stress level (Eq. 64b). Less is known on how water stress exactly affects trunk height. Nonetheless, trunk height measurements by Foong (1999) revealed that irrigated mature palms in 148 palms ha^{-1} were taller by an average 9% than non-irrigated palms with the same planting density and age. Eq. 88 was developed to reflect this effect.

Measurements of the canopy or crown height for oil palm trees aged between 1 and 20 years (N = 12) gave the following linear regression:

$$h_{canopy} = 1.5091 + 0.001382 age. \quad (89)$$

Canopy height was measured from the base of frond 41 to the tip of frond 1, so, although the rachis length will finally plateau with tree age, our measurements revealed that the length or vertical distance between the base of frond 41 and frond 1 increased in a linear manner. Consequently, tree height h (m) is the summation of trunk height h_{trunk} and canopy height h_{canopy}.

Lastly, the increase in rooting depth d_{root} between two successive time steps t and t+1 is

$$d_{root,t+1} = d_{root,t} + \left(dg_{root} \times R_{Dc}\right) \quad (90)$$

where dg_{root} is the daily increase in the rooting depth, taken as 0.002 m day^{-1}, the mean value of root growth for oil palm (Henson and Chai 1997; Jourdan and Rey 1997), and root growth is detrimentally affected by water stress R_{Dc} (Kropff 1993). Note that rooting depth will not exceed the maximum soil depth set in the model.

8 Model testing

The accuracy of the PySawit model was evaluated by comparing its simulations with several measured growth and yield parameters of oil palm in Merlimau estate (2.253213°N, 102.451753°E), Melaka. The Merlimau data set is independent and not part of the other data sets used during the development of the PySawit model.

At Merlimau, commercial dura x pisifera (Deli x AVROS) palms were planted at the following densities: 120, 135, 148, 164, 181, 199, 220, 243, 268 and 296 palms ha^{-1}. Field plantings for all densities were simultaneously done on April 1987 when the palms were 1 year old. At field planting, the mean (± s.e.) initial dry weights (kg DM palm^{-1}) for the palm parts pinnae, rachis, trunk and roots were 0.40 ± 0.07, 0.70 ± 0.11, 0.10 ± 0.01 and 0.20 ± 0.03, respectively. Field measurements continued every year until the palms were 19 years old (December 2006). Non-destructive methods by Corley and Tinker (2016), Breure (2003), Corley et al. (1971) and Hardon et al. (1969) were used to estimate leaf area and dry weights of frond (inclusive of pinnae, rachis and petiole) of oil palms. These are the oil palm industry standard methods which are currently being used to estimate the crop's dry matter production. At palm maturity stage, the fertilizers applied were ammonium sulphate, muriate of potash, rock phosphate and kieserite at rates 3.5, 3.5, 2.0 and 1.25 kg palm^{-1} yr^{-1}, respectively.

The soil type at Merlimau is a sandy clay loam Rengam soil series (Typic Paleudults), and the first 0.45 m soil depth has a mean (± s.e.) clay, sand, organic C and total N contents of 27.4 ± 0.7, 67.3 ± 0.8, 1.7 ± 0.1 and 0.14 ± 0.01%, respectively. Available soil water content was, however, not measured.

PySawit required the following model inputs to be supplied: site latitude; daily weather (minimum and maximum air temperatures, wind speed, and rainfall amount); N and mineral contents in the individual plant parts of the oil palm tree, as well as the specific leaf area *SLA* (data obtained from van Kraalingen et al. 1989); soil properties (sand, clay, and organic matter contents); and the initial dry weights of the individual plant parts.

Three goodness-of-fit statistical indexes were used to summarize the degree of agreement between PySawit's predictions and observations. These indexes were Normalized Mean Bias Error (NMBE), Normalized Mean Absolute Error (NMAE) and the revised Willmott's index of agreement (d_r) (Willmott et al. 2012; Yu et al. 2006). These indexes are calculated as follows:

$$NMBE = \frac{\sum_{i=1}^{N} P_i - O_i}{\sum_{i=1}^{N} O_i} \tag{91}$$

$$NMAE = \frac{\sum_{i=1}^{N} |P_i - O_i|}{\sum_{i=1}^{N} O_i} \tag{92}$$

$$d_r = \begin{cases} 1 - p/2o & p \le 2o \\ 2o/p - 1 & p > 2o \end{cases} \tag{93a}$$

$$p = \sum_{i=1}^{N} |P_i - O_i| \quad \text{and} \quad o = \sum_{i=1}^{N} O_i - \bar{O} \tag{93b}$$

where P_i and O_i are the i-th pair of predicted and observed values, respectively (i = 1 to N pairs); and $\bar{O}$ is the mean of all observed values. NMBE (−1 to $+\infty$) indicates a model's tendency to under- or overestimate relative to the mean observations. The larger the NME value, the larger the model's tendency for overestimation. NMAE (0 to $+\infty$) indicates the mean absolute difference between predicted and observed values relative to the mean observations. Larger NMAE values indicate larger mean departures between model predictions and observations. The revised index of agreement d_r ranges between −1 and +1, where increasingly smaller positive or larger negative values indicate increasingly worse or inaccurate model predictions (particularly when $d_r < 0$). For a perfect model, NMBE = 0 (no overall model bias), NMAE = 0 and d_r = +1 (the latter two indicating perfect agreement between model predictions and observations).

9 Results and discussion

The mean (± s.e.) minimum and maximum air temperatures recorded at Merlimau from 1987 to 2006 were 23.71 ± 0.01 and 32.19 ± 0.03°C, respectively. Mean daily wind speed was 1.60 ± 0.01 m s^1 and the mean daily total solar irradiance was 19.27 ± 0.02 MJ m^{-2}.

Mean annual rainfall was 1918 ± 12 mm, with two notable dry years which occurred during 1997–8 and 2004–5 (year 11 and 18 of field planting, respectively), both of which corresponded to the occurrence of El Niño. The amount of rain received for 1997–8 and 2004–5 were 15 and 32% less than the average annual rainfall at Merlimau, respectively.

Overall, PySawit showed good agreement, with little to no bias, in predicting the growth and yield parameters of oil palm (Fig. 11 to 17). Predictions were especially good for TDM,

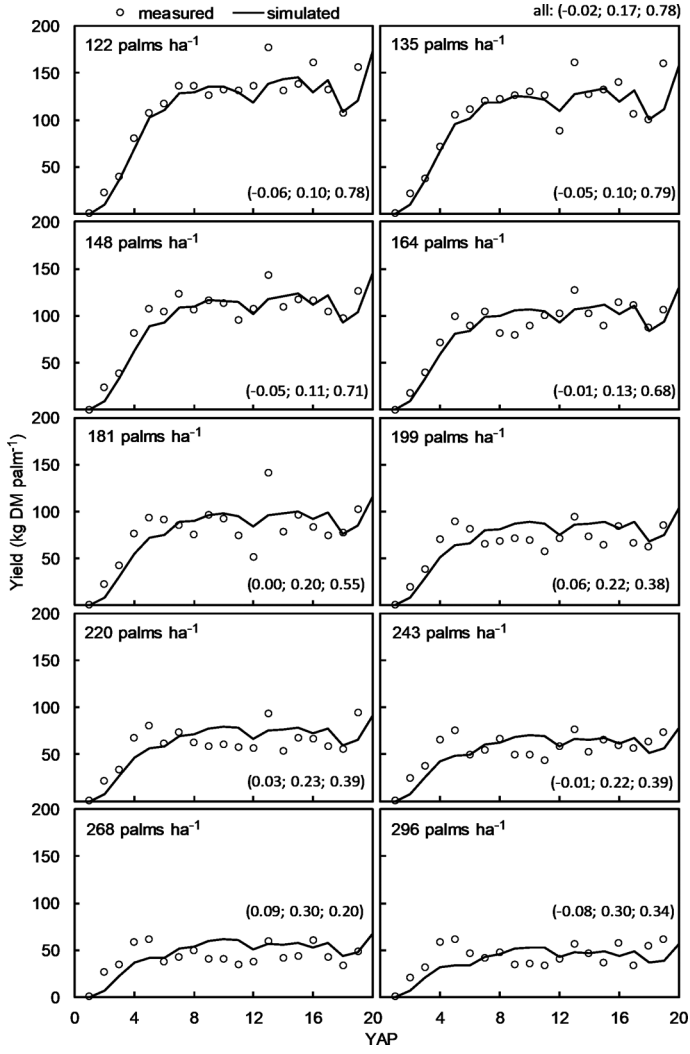

Figure 11 Comparisons between model simulations and observations for fresh fruit bunch (FFB) yield. Years 11 and 18 recorded El Niño events. Values in brackets denote NMBE, NMAE and d_r, where NMBE is the normalized mean bias error, NMAE is the normalized mean absolute error and d_r is the revised index of agreement. YAP is year after planting.

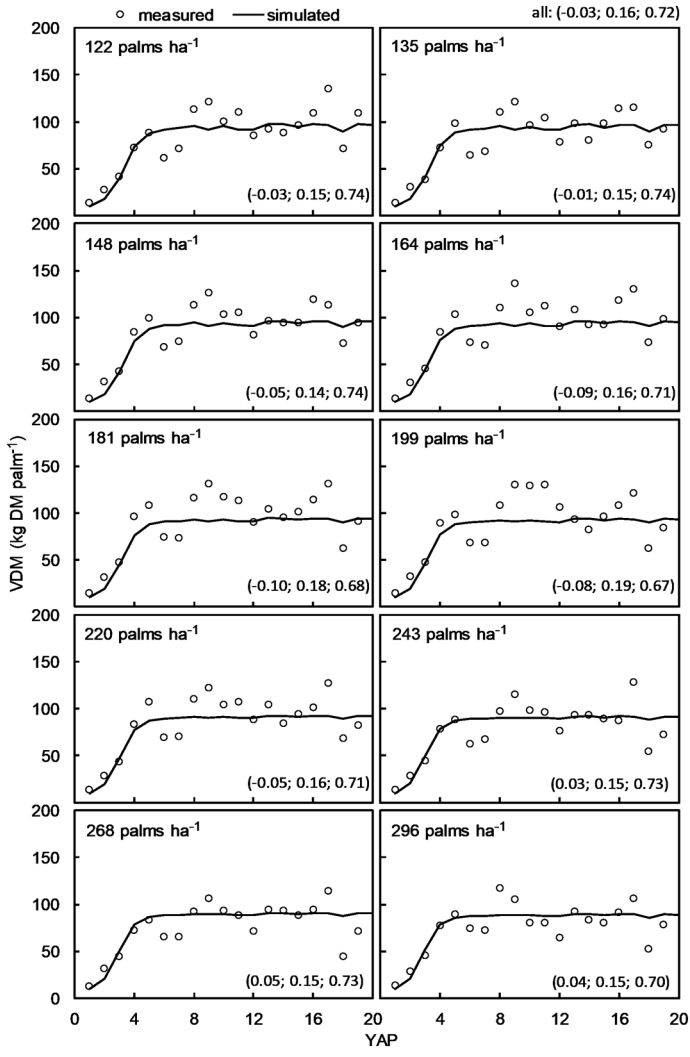

Figure 12 Comparisons between model simulations and observations for aboveground vegetative dry matter (VDM). Values in brackets denote NMBE, NMAE and d_r, where NMBE is the normalized mean bias error, NMAE is the normalized mean absolute error and d_r is the revised index of agreement. YAP is year after planting.

LAI and trunk height, as indicated by their small NMAE values (≤13%), large positive d_r values (>0.8) and near zero NMBE values. Moreover, model accuracy remained stable across all planting densities.

However, discrepancies between yield predictions and observations were found to increase with increasing planting density (Fig. 11). Yield prediction for planting density 122 palms ha^{-1} (PD122), for instance, had a high d_r value of 0.78, but this declined to

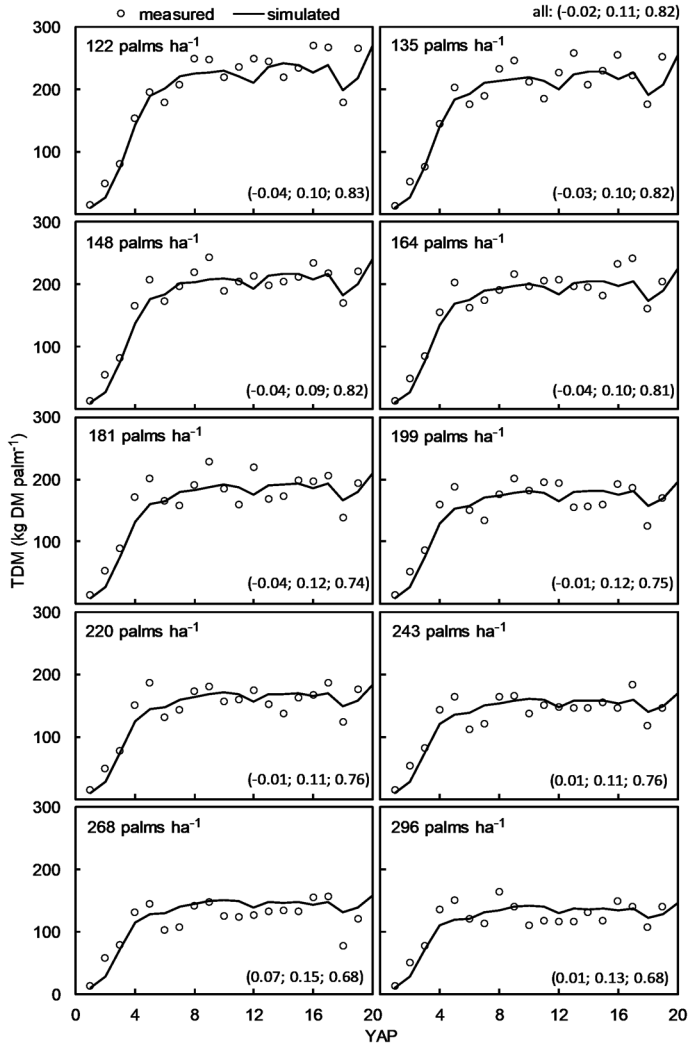

Figure 13 Comparisons between model simulations and observations for total dry matter (TDM), which is the sum of yield and aboveground vegetative dry matter (VDM). Values in brackets denote NMBE, NMAE and d_r, where NMBE is the normalized mean bias error, NMAE is the normalized mean absolute error and d_r is the revised index of agreement. YAP is year after planting.

0.34 for PD296. The degree of model bias also increased with increasing planting density. Nonetheless, paired sample t-test showed no significant differences (p>0.05) between yield predictions and observations across all planting densities, even for PD296, although the level of significance generally declined with increasing planting density. For instance, yield predictions for PD122 was significantly different from observations only at 62% level of significance, but for PD296, this level of significance was 10%.

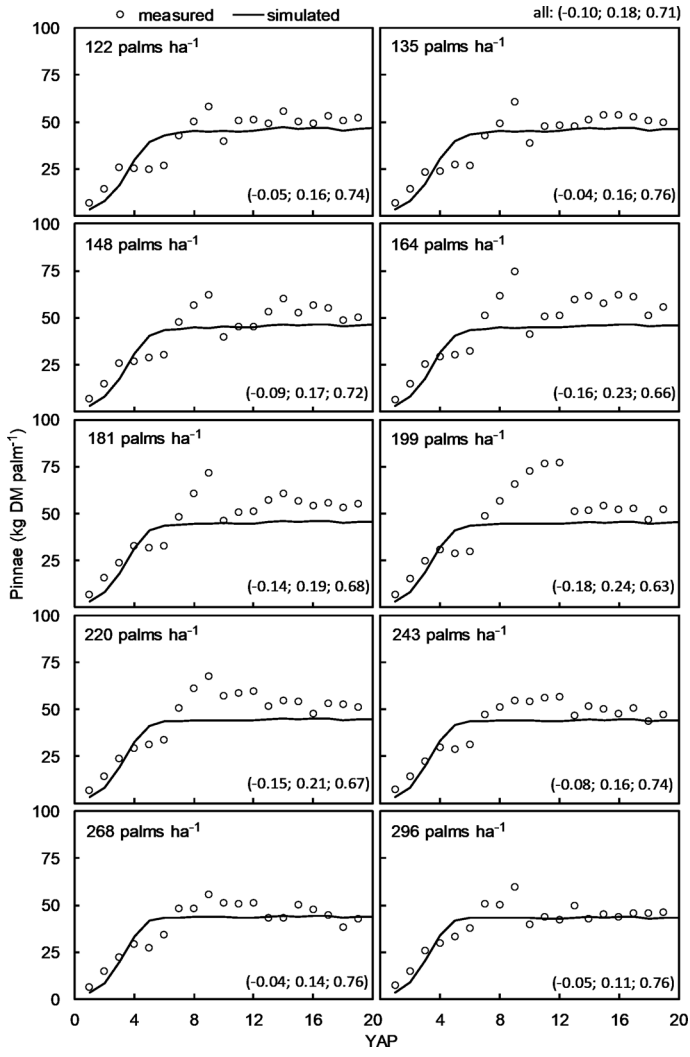

Figure 14 Comparisons between model simulations and observations for pinnae biomass. Values in brackets denote NMBE, NMAE and d_r, where NMBE is the normalized mean bias error, NMAE is the normalized mean absolute error and d_r is the revised index of agreement. YAP is year after planting.

Both years 11 and 18 recorded El Niño events which caused oil palm yields to decline in year 12 (one year after the first El Niño event) and year 18 (the same year as the second El Niño event). Relative to the mean yields from year 10 to 19, yields from all planting densities were reduced by an average (± s.e.) of 12.7 ± 4.3 and 11.6 ± 4.4% in years 12 and 18, respectively. Model simulations also showed a likewise decline in yields for both these years: by an average (± s.e.) of 8.6 ± 0.3% in year 12 and 18.2 ± 0.3% in year 18 (Fig. 11). Yield simulations for mature palms (years 10 to 19) remained rather stable, where the

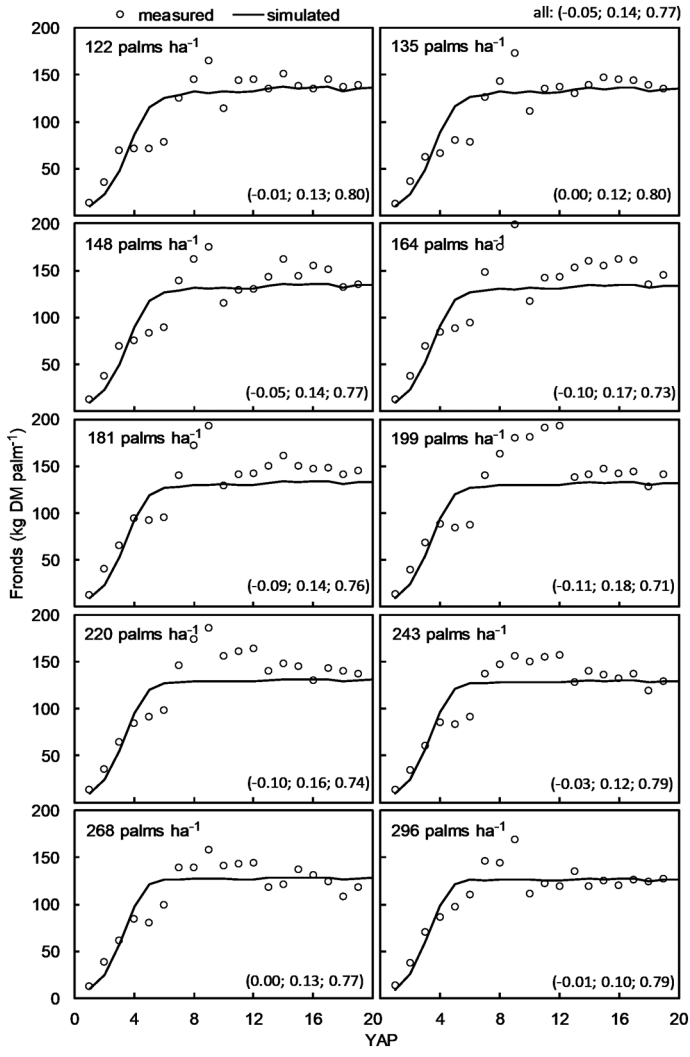

Figure 15 Comparisons between model simulations and observations for fronds (pinnae and rachis) biomass. Values in brackets denote NMBE, NMAE and d_r, where NMBE is the normalized mean bias error, NMAE is the normalized mean absolute error and d_r is the revised index of agreement. YAP is year after planting.

goodness-of-fit indexes for mature oil palm yield simulations were: 0.03 for NMBE, 0.17 for NMAE and 0.77 for d_r, only a slight decrease compared to yield simulations for all palm ages (year 2 to 19).

The large variations in the measured aboveground VDM for all planting densities especially year 5 onwards (Fig. 12) are unlikely to be real, and they suggest large measurement errors in the field. Nevertheless, model simulations showed a much more

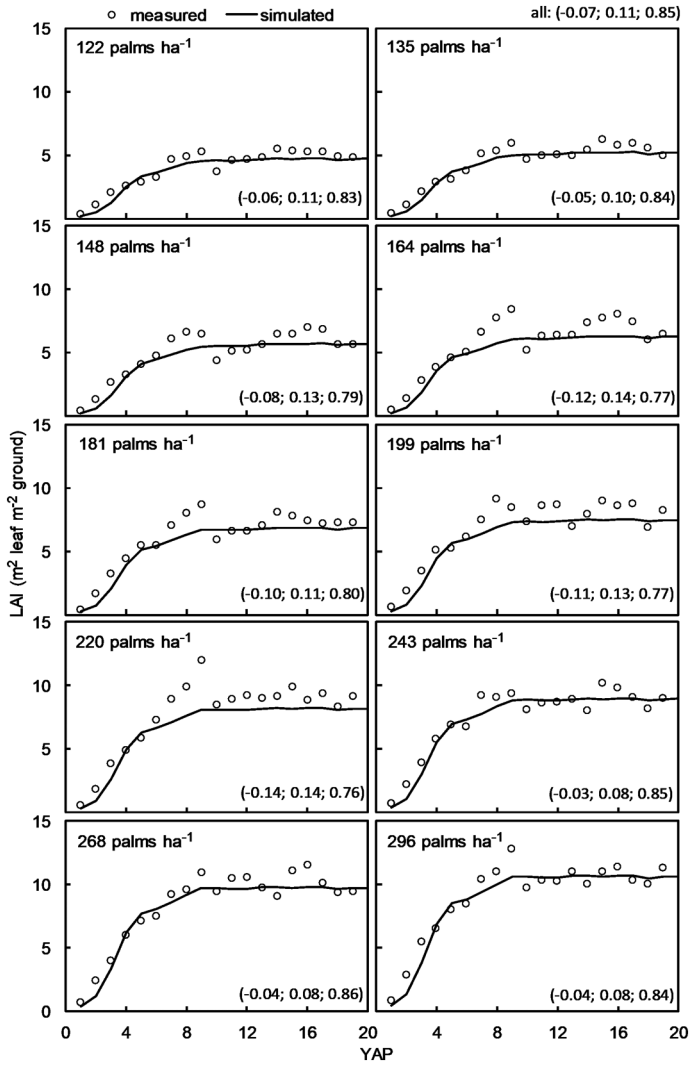

Figure 16 Comparisons between model simulations and observations for total leaf area index (LAI). Values in brackets denote NMBE, NMAE and d_r, where NMBE is the normalized mean bias error, NMAE is the normalized mean absolute error and d_r is the revised index of agreement. YAP stands for the year after planting.

steady temporal trend, and the *mean* of measured VDM from years 5 to 19 agreed closely with the model simulations for the same period.

Simulations also revealed that at Merlimau, plant water deficit increased with increasing planting density. In PD122, the mean annual plant water deficit was 218 mm but in PD296, the deficit was 350 mm. Mean annual plant water deficit increased by average of 7 mm for every 10 palms ha^{-1} increase in planting density.

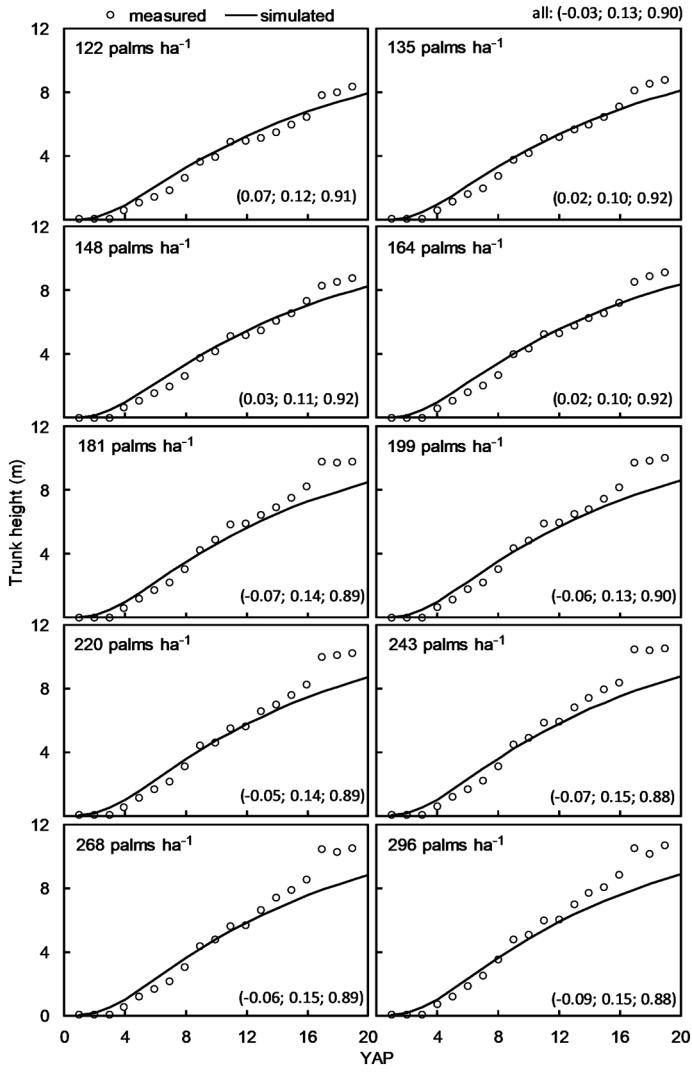

Figure 17 Comparisons between model simulations and observations for trunk height. Values in brackets denote NMBE, NMAE and d_r, where NMBE is the normalized mean bias error, NMAE is the normalized mean absolute error and d_r is the revised index of agreement. YAP stands for the year after planting.

It is well established that crops in higher planting densities will produce lower yields and biomass on a per plant basis than in lower planting densities. Specifically for oil palm, PySawit revealed that mean gross photosynthesis in PD122 was 878 kg CH_2O palm^{-1}, of which nearly two-thirds (65%) of the assimilates were used for total (maintenance and growth) respiration. The balance of the assimilates (35% or about 303 kg CH_2O palm^{-1}) was then available for flower and bunch development. But the mean gross photosynthesis

rate for the highest planting density of PD296 was at a lower level of 624 kg CH_2O $palm^{-1}$ (29% lower than in PD122), but total respiration consumed 83% of the assimilates, leaving only 17% (105 kg CH_2O $palm^{-1}$, which is about a third less than that used in PD122) for flower and bunch development.

There are several reasons for the lower gross photosynthesis at higher than lower planting densities, one of which is the increase in the proportion of shaded to sunlit canopies at higher planting densities compared with that at the lower planting densities. Increasing the proportion of shaded to sunlit canopies by 30%, for instance, lowers gross photosynthesis by nearly the same percentage (see Eq. 11). Increased leaf area at higher planting densities would also increase the wind speed extinction coefficient, thus reducing air flow within and below the canopies. In turn, this results in lower gas exchanges and lower photosynthetic rates.

Although many studies have been carried out on oil palm, there remain considerable gaps in knowledge, one of which relates to the microclimate conditions under the oil palm canopies. Much less is known about the vertical wind speed profile and how soil water content and plant water uptake differ between oil palm planting densities. The accurate method of scaling up leaf to canopy conductance also needs to be studied in greater detail. Knowledge of these properties would allow oil palm models to better portray the daily variability of microclimate conditions under the oil palm canopies and to produce yield predictions that better match the variability or fluctuations in observed yields. That PySawit's yield prediction errors would become increasingly large for increasingly higher planting densities is indicative that the model's characterization of the microclimate conditions particularly under very dense canopies is still not representative enough. More work is also needed to determine the effects of planting density on the dry matter and nutrient content partitioning between the individual tree parts of oil palm.

10 Conclusion

An oil palm growth and yield model (PySawit) for crop production level 2 (where growth is only limited by weather conditions and water) was successfully developed. PySawit mainly differs from other oil palm models in several aspects. PySawit models photosynthesis in a more rigorous, physically based manner, by including, among others, actual oil palm leaf measurements to determine the temporal change in maximum Rubisco capacity rate and intercellular concentration of CO_2. The plant–atmosphere–soil of the oil palm system was modelled as a network of resistances to solve the energy balance of the system. Actual measurements to determine the relationship between oil palm leaf stomatal conductance with PAR and VPD were additionally used. This allowed us to determine the simultaneous loss of water via oil palm transpiration and soil evaporation.

An independent data set from Merlimau oil palm trials (with various planting densities) was used to evaluate PySawit's accuracy. Model predictions generally agreed with observed values for several growth and yield parameters, and model accuracy was stable across all planting densities. Model predictions were especially good (small discrepancies between predictions and observations and very little to none model bias) for TDM, LAI and trunk height parameters. Yield decreases due to two El Niño events (which caused dry periods) were also reflected well in the model simulations. However, discrepancies between yield predictions and observations increased with increasing planting density. This is possibly because the

microclimate conditions particularly under very dense canopies is not well understood and insufficiently characterized by the model. More work is also needed to determine the effects of planting density on soil water content, plant water use and dry matter and nutrient content partitioning between the individual tree parts. Knowledge of these properties would further improve the model's accuracy and extend its range of applications.

PySawit was implemented as a computer program using Python computer language. The source code for PySawit can be downloaded from www.christopherteh.com/pysawit.

11 Where to look for further information

The following is a list of several possible directions for future research: 1) to measure the daily soil water content, soil evaporation and oil palm transpiration under different planting densities, 2) to determine the vertical wind speed profile above and below oil palm canopies and 3) to model the uptake of nutrients by oil palm and their effect on the tree growth and yield.

Universiti Putra Malaysia (UPM), one of 20 public universities in Malaysia, has 16 faculties, one of which is the oldest faculty, the Faculty of Agriculture. This faculty comprises seven departments: Crop Science, Plant Protection, Land Management, Animal Science, Agribusiness and Bioresource Economics, Agriculture Technology and Aquaculture. These departments were established based on the concept of unification or integration of the key elements in the agricultural system: plants, animals, soil, technology and management.

Sime Darby Plantation has been involved in agriculture research and development since the early 1900s. Areas of research include best management practices, zero burning replanting techniques, oil palm nutrition, water conservation and irrigation, Integrated Pest Management, and the conversion of Empty Fruit Bunches and Palm Oil Mill Effluent into compost. Sime Darby Plantation is also involved in the sequencing, assembling and annotating the oil palm genome.

12 Acknowledgement

The authors would like to thank Sime Darby Research Sdn. Bhd. for permission to use the oil palm trial and weather data for this modelling study.

13 List of main symbols

Symbol	Description	Units
γ	psychometric constant (0.658)	mbar K^{-1}
Γ^*	CO_2 compensation point	μmol CO_2 mol^{-1} air
Δ	slope of the saturated vapour pressure curve	mbar K^{-1}
θ	solar inclination (from vertical)	radians

θ	volumetric soil water content	$m^3\ m^{-3}$
$\theta_{0/33/1500}$	volumetric soil water content at saturation (0), field capacity (33), or permanent wilting point (1500)	$m^3\ m^{-3}$
θ_{root}	volumetric soil water content in the root zone	$m^3\ m^{-3}$
θ_{cr}	critical volumetric soil water content	$m^3\ m^{-3}$
Θ_i	soil water content	m
λ	pore-size distribution index	–
λET	total latent heat flux density	$W\ m^{-2}$
$\lambda ET_{c/s}$	latent heat flux density of crop (c) or soil (s)	$W\ m^{-2}$
Λ_{canopy}	instantaneous gross canopy assimilation	μmol CO_2 m^{-2} ground s^{-1}
$\Lambda_{canopy,d}$	daily gross canopy assimilation	kg CH_2O $palm^{-1}$ day^{-1}
$\Lambda_{sl/sh}$	gross leaf assimilation rate of CO_2 for sunlit (sl) or shaded (sh) leaves	μmol CO_2 m^{-2} leaf s^{-1}
$\rho_{df/dr}$	reflection coefficient for diffuse (df) or direct photosynthetically active radiation (PAR)	–
ρc_p	volumetric heat capacity of air (1221.09)	$J\ m^{-3}\ K^{-1}$
τ	CO_2 / O_2 specificity factor	μmol O_2 μmol^{-1} CO_2
τ	atmospheric transmittance (sky clearness)	–
τ	soil tortuosity	–
τ_b	canopy gap fraction	–
ϕ_p	soil porosity	$m^3\ m^{-3}$
ω, ω_0	canopy clustering coefficient at current sun position and at when the sun is at zenith, respectively	–
age	tree age	days
A	total energy supply to crop and soil	$W\ m^{-2}$
$A_{c/s}$	energy available to the crop (c) or soil (s)	$W\ m^{-2}$
$C_{a/i}$	CO_2 concentration in ambient air (a) and within stomata (i)	μmol CO_2 mol^{-1} air
CVF, CVF_2	conversion from CH_2O to dry (DM) weight	kg DM kg^{-1} CH_2O
d	zero plane displacement	M
d_{root}	rooting depth	m
dg_{root}	rooting depth growth rate	$m\ day^{-1}$
D	air vapour pressure deficit (VPD)	mbar
$D_{0/leaf}$	air VPD at mean canopy flow (0) or leaf VPD (leaf)	mbar
DL	day length	hour

$DM_{(part)}$	fraction of dry matter to a given plant part	–
e_a	air vapour pressure	mbar
e_m	quantum efficiency or yield (0.051)	μmol CO_2 $μmol^{-1}$ photons
$e_s[\![T]\!]$	saturated vapour pressure at temperature T	mbar
$ET_{c/s}$	potential transpiration (c) or evaporation (s)	m day^{-1}
$f_{D/PAR/water}$	reduction of stomatal conductance due to VPD (D), low PAR, or water stress (water)	–
gst, gst_{max}	current and maximum stomatal conductance, respectively	m s^{-1}
G	soil (ground) heat flux density	W m^{-2}
$G_{death,(part)}$	death rate of a given plant part	kg DM $palm^{-1}$ day^{-1}
G_{gen}	total assimilates available for generative organs growth	kg CH_2O $palm^{-1}$ day^{-1}
$G_{gen,\ (part)}$	growth rate of a given generative organ	kg DM $palm^{-1}$ day^{-1}
G_{growth}	total assimilates available for vegetative growth respiration	kg CH_2O $palm^{-1}$ day^{-1}
$G_{growth,\ (part)}$	growth rate of a given plant part	kg DM day^{-1}
h	tree height (trunk + canopy)	M
h_{canopy}, h_{trunk}	canopy and trunk height, respectively	m
h'_{trunk}	rate of growth for trunk height	m day^{-1}
H	total head (matric and gravity)	M
H	total sensible heat density	W m^{-2}
$H_{c/s}$	sensible heat flux density of crop (c) or soil (s)	W m^{-2}
$I_{df/dr}$	diffuse (df) or direct (dr) solar irradiance	W m^{-2}
I_{et}, I_t	extraterrestrial and total solar irradiance, respectively	W m^{-2}
k	von Karman's constant (0.4)	–
$k_{df/dr}$	canopy extinction coefficient for diffuse (df) or direct (dr) solar radiation	–
$k_{e/w}$	extinction coefficient for eddy diffusivity (e) or wind speed (w)	–
K_θ, $\overline{K_\theta}$	unsaturated and mean hydraulic conductivity, respectively	m day^{-1}
$K_{c/o}$	Michaelis–Menten constant for CO_2 (c) or O_2 (o)	μmol CO_2/O_2 mol^{-1} air
L, L_{eff}	total and effective leaf area index, respectively	m^2 leaf m^{-2} ground
$L_{sh/sl}$	shaded (sh) or sunlit (sl) leaf area index	m^2 leaf m^{-2} ground

$L_{max,PD}$	maximum leaf area index for a given planting density	m^2 leaf m^2 ground
m	optical mass number	–
$M_{(part)}$	maintenance respiration for a given plant part	kg CH_2O $palm^{-1}$ day^{-1}
$N_{(part)}$	fraction by weight of nitrogen content in given plant part	–
O_a	air ambient concentration of O_2	µmol O_2 mol^{-1} air
PD	planting density	palms ha^{-1}
P_g, P_{net}	gross and net daily rainfall, respectively	M
q	water flux	m day^{-1}
$\widehat{q_i}$	net water flux	m day^{-1}
$Q_{df/dr}$	diffuse (df) or direct (dr) PAR component	µmol m^{-2} leaf s^{-1}
$Q_{sh/sl}$	total PAR absorbed by shaded (sh) or sunlit (sl) leaves	µmol m^{-2} leaf s^{-1}
Q_{10}	relative change for every 10 °C change	–
$\overline{Q_{p,df}}$	mean diffuse PAR component (within canopies)	µmol m^{-2} ground s^{-1}
$Q_{p,dr}$	unintercepted direct PAR component (with scattering component) (within canopies)	µmol m^{-2} leaf s^{-1}
$Q_{p,dr,\alpha}$	scattered PAR component only (within canopies)	µmol m^{-2} ground s^{-1}
$Q_{p,dr,dr}$	unintercepted direct PAR component (without scattering component) (within canopies)	µmol m^{-2} leaf s^{-1}
	aerodynamic resistance between the mean canopy flow and reference height	s m^{-1}
	bulk boundary layer resistance	s m^{-1}
	canopy resistance	s m^{-1}
	aerodynamic resistance between the soil surface and mean canopy flow	s m^{-1}
	soil surface resistance	s m^{-1}
R_n, R_{nL}	net solar radiation and net long-wave radiation, respectively	W m^{-2}
R_{Ds}, R_{Dc}	reduction factor for evaporation and transpiration, respectively	–
RH	relative humidity	%
SLA	specific leaf area	m^2 leaf kg^{-1} DM
t_h	local solar hour	Hour
t_{sr}, t_{ss}	local solar hour for sunrise and sunset, respectively	Hour
T_a, T_{dew}, T_f	air, dew point and foliage temperature, respectively	°C
$T_{min/max}$	minimum (min) or maximum (max) air temperature	°C

u_*	friction velocity	m s^{-1}
u, u_d, u_h	wind speed, mean daily wind speed and wind speed at canopy height, respectively	m s^{-1}
$u_{min/max}$	minimum (min) or maximum (max) daily wind speed	m s^{-1}
$v_{c/q/s}$	CO_2 assimilation limited by Rubisco (c), light (q), or sink (s)	μmol CO_2 m^{-2} leaf s^{-1}
V_{cmax}	Rubisco capacity rate	μmol CO_2 m^{-2} leaf s^{-1}
VDM, $VDM_{max,PD}$	current and maximum vegetative dry matter requirement for a given planting density, respectively	kg DM $palm^{-1}$ yr^{-1}
w	mean pinnae width	m
$W_{(part)}$	dry weight of a given plant part	kg DM $palm^{-1}$
$X_{(part)}$	fraction by weight of mineral content in a given plant part	–
$z_{0/s0}$	crop (0) or soil surface (s0) roughness length	m
z_r	reference height	m

14 References

Awal, M. A. (2008). Assessment of gap fraction by hemispherical photograph in oil palm plantation. *Suranaree Journal of Science and Technology*, 15, 233–41.

Bentley, A. (2007). *Interception loss in Sedenak oil palm plantation*. B.Sc. final year project report. Skudai, Malaysia: Universiti Teknologi Malaysia.

Bernacchi, C. J., Portis, A. R., Nakano, H., von Caemmerer, S. and Long, S. P. (2002). Temperature response of mesophyll conductance. Implication for the determination of Rubisco enzyme kinetics and for limitations to photosynthesis *in vivo*. *Plant Physiology*, 130, 1992–8.

Bernacchi, C. J., Singsaas, E. L., Pimentel, C., Portis Jr., A. R. and Long, S. P. (2001). Improved temperature response functions for models of Rubisco-limited photosynthesis. *Plant, Cell and Environment*, 24, 253–9.

Bittelli, M., Campbell, G. S. and Tomeu, F. (2015). *Soil Physics with Python. Transport in the Soil-Plant-Atmosphere System*. Oxford, UK: Oxford University Press.

Breure, C. J. (2003). The search for yield in oil palm: Basic principles. In T. H. Fairhurst and R. Härdter (Eds.), *Oil Palm: Management for Large and Sustainable Yields* (pp. 59–98). Singapore: Potash & Phosphate Institute of Canada (ESEAP).

Breure, C. J. and Powell, M. S. (1988). The one-shot method of establishing growth parameters in oil palm. In H. A. Halim, P. S. Chew and B. J. Wood (Eds.), *Proceedings of the 1987 International Oil Palm Conference. Progress and prospects* (pp. 203–9). Kuala Lumpur, Malaysia: Palm Oil Research Institute of Malaysia.

Brutsaert, W. (1982). *Evaporation into the Atmosphere. Theory, History and Applications*. Dordrecht, The Netherlands: D. Reidel Publishing Company.

Campbell, G. S. and Norman, J. M. (1998). *An Introduction to Environmental Biophysics* (2nd ed.). New York, NY: Springer-Verlag.

Chong, S. Y. (2012). *Development of Simple Equations to Estimate the Net Rainfall Under Closed Tree Canopies*. M. Agr. Sc. dissertation. Serdang, Malaysia: Universiti Putra Malaysia.

Choudhury, B. J. and Monteith, J. L. (1988). A four-layer model for the heat budget of homogeneous land surfaces. *Quarterly Journal of the Royal Meteorological Society*, 114, 373–98.

Collatz, G. T., Ball, J. T., Grivet, C. and Berry, J. A. (1991). Physiological and environmental–regulation of stomatal conductance, photosynthesis and transpiration: A model that includes a laminar boundary layer. *Agricultural and Forest Meteorology*, 54, 107–36.

Combres, J. -C., Pallas, B., Rouan, L., Mialet-Serra, I., Caliman, J. -P., Braconnier, S., Soulié, J. -C. and Dingkuhn, M. (2012). Simulation of inflorescence dynamics in oil palm and estimation of environment-sensitive phenological phases: A model based analysis. *Functional Plant Biology*, 40, 263–79.

Corley, R. H. V. and Tinker, P. B. (2016). *The Oil Palm* (5th ed.). Chichester, UK: Wiley-Blackwell.

Corley, R. H. V., Hardon, J. J. and Tan, G. Y. (1971). Analysis of growth of the oil palm (*Elaeis guineensis* Jacq.) I. Estimation of growth parameters and application in breeding. *Euphytica*, 20, 307–15.

Corley, R. H. V., Ng, M. and Donough, C. R. (1995). Effects of defoliation on sex differentiation in oil palm clones. *Experimental Agriculture*, 31, 177–89.

Damih, A. 1995. *Keberkesanan pemintasan air hujan oleh pokok kelapa sawit di dalam mengurangkan air larian permukaan* [Effectiveness of rainfall interception by oil palm trees in reducing surface runoff]. B.Sc. final year project report. Skudai, Malaysia: Universiti Teknologi Malaysia.

de Wit, C. T. and Penning de Vries, F. W. T. (1982). L'Analyse des systemes de production primaire [Analysis of primary production systems]. In F. W. T. Penning de Vries and M. A. Djiteye (Eds.), *Une etude des sols, des vegetations et de l'exploitation de cette ressource naturelle* [A study of the soils, vegetations and exploitation of this natural resource] (pp. 20–27). Agricultural Research Reports 918. Wageningen, The Netherlands: Pudoc.

Dimas, F. A., Gilani, S. I. H. and Aris, M. S. (2011). Hourly solar radiation estimation using ambient temperature and relative humidity data. *International Journal of Environmental Science and Development*, 2, 188–93.

Dufrêne, E. and Saugier, B. (1993). Gas exchange of oil palm in relation to light, vapour pressure deficit, temperature and leaf age. *Functional Ecology*, 7, 97–104.

Dufrêne, E., Ochs, R. and Saugier, B. (1990). Oil palm photosynthesis and productivity linked to climatic factors. *Oléagineux*, 45, 345–55.

Ephrath, J. E., Goudriaan, J. and Marani, A. (1996). Modelling diurnal patterns of air temperature, radiation, wind speed and relative humidity by equations from daily characteristics. *Agricultural Systems*, 51, 377–93.

Fan, Y., Roupsard, O., Bernoux, M., Le Maire, G., Panferov, O., Kotowska, M. M. and Knohl, A. (2015). A sub-canopy structure for simulating oil palm in the Community Land Model (CLM-Palm): phenology, allocation and yield. *Geoscientific Model Development*, 8, 3785–3800.

Farahani, H. J. and Ahuja, L. R. (1996). Evapotranspiration modeling of partial canopy/residue-covered fields. *Transactions of the ASAE*, 39, 2051–64.

Farquhar, G. D., von Caemmerer, S. and Berry, J. A. (1980). A biochemical model of photosynthetic CO_2 assimilation in leaves of C3 species. *Planta*, 149, 78–90.

Foong, F. S. (1999). Impact of moisture on potential evapotranspiration, growth and yield of oil palm. In D. Arifin, K. W. Chan and S. R. S. A. Sharifah (Eds.), *Proceedings of the 1999 PORIM International Palm Oil Congress (Agriculture)* (pp. 265–87). Bangi, Malaysia: Palm Oil Research Institute of Malaysia.

Gerritsma, W. (1988). *Simulation of oil palm yield*. Report. Department of Theoretical Production Ecology. Wageningen, The Netherlands: Wageningen Agricultural University.

Goudriaan, J. (1977). *Crop micrometeorology: A simulation study*. Simulation Monograph. Pudoc, Wageningen: Centre for Agricultural Publishing and Documentation.

Goudriaan, J. and van Laar, H. H. (1994). *Modeling Potential Crop Growth Processes. A Textbook with Exercise*. Current issues in production ecology. Dordrecht, The Netherlands: Kluwer Academic Publishers.

Hansen, F. V. (1993). *Surface Roughness Lengths*. ARL Technical Report. White Sands Missile Range, NM 88002-5501: U.S. Army.

Hardon J. J., Williams C. N. and Watson I. (1969). Leaf area and yield in the oil palm in Malaya. *Experimental Agriculture*, 5, 25–32.

Hasanuzzaman, M., Nahar, K., Alam, M. M., Roychowdhury, R. and Fujita, M. (2013). Extreme temperature responses, oxidative stress and antioxidant defense in plants. In K. Vahdat and C. Leslie (Eds.), *Abiotic Stress – Plant Responses and Applications in Agriculture* (pp. 169–205). Vienna, Austria: InTech.

Henry, P. (1955). Leaf growth morphology in Elaeis. *Revue Generale de Botanique*, 32, 66–7.

Henson, I. E. (1989). *Modelling Gas Exchange, Yield and Conversion Efficiency*. Workshop on Productivity of Oil Palm. Bangi, Malaysia: Palm Oil Research Institute of Malaysia.

Henson, I. E. (1995). Carbon assimilation, water use and energy balance of an oil palm plantation assessed using micrometeorological techniques. In S. Jalani, D. Ariffin, N. Rajanaidu, D. Mohd Tayeb, K. Paranjothy, W. Mohd Basri, I. E. Henson and C. K. Chan (Eds.), *Proceedings of the 1993 PORIM International Palm Oil Congress – Update and Vision (Agriculture)* (pp. 137–58). Bangi, Malaysia: Palm Oil Research Institute of Malaysia.

Henson, I. E. (2000). Modelling the effects of 'haze' on oil palm productivity and yield. *Journal of Oil Palm Research*, 12, 123–34.

Henson, I. E. (2006). OPFLSIM3 – An improved oil palm seasonal flowering and yield simulation model. *Oil Palm Bulletin*, 53, 1–24.

Henson, I. E. (2009). Modelling dry matter production, partitioning and yield of oil palm. OPRODSIM: A mechanistic simulation model for teaching and research. Technical manual and users' guide. Kuala Lumpur, Malaysia: Malaysian Palm Oil Board.

Henson, I. E. and Chai, S. (1997). Analysis of oil palm productivity. II. Biomass, distribution, productivity and turnover of the root system. *Elaeis*, 9, 78–92.

Henson, I. E. and Mohd Tayeb, D. (2003). Physiological analysis of an oil palm density trial on a peat soil. *Journal of Oil Palm Research*, 15, 1–27.

Hillel, D. (1977). *Computer Simulation of Soil-water Dynamics: A Compendium of Recent Work*. Ottawa, Canada: International Development Research Centre.

Hoffmann, M. P., Castaneda Vera, A., van Wijk, M. T., Giller, K. E., Oberthür, T., Donough, C. and Whitbread, A. M. (2014). Simulating potential growth and yield of oil palm (*Elaeis guineensis*) with PALMSIM: Model description, evaluation and application. *Agricultural Systems*, 131, 1–10.

Huth, N. I., Banabas, M., Nelson, P. N. and Webb, M. (2014). Development of an oil palm cropping systems model: lessons learned and future directions. *Environmental Modelling & Software*, 62, 411–19.

Jacquemard, J. C. (1979). Contribution to the study of the height growth of the stems of Elaeis guineensis Jacq. Study of the L2T x D10D cross. *Oléagineux*, 34, 492–7.

Jacquemard, J. C. (1998). *Oil palm*. London, UK: Macmillan Education Ltd.

Jourdan, C. and Rey, H. (1997). Architecture and development of the oil-palm (*Elaeis guineensis* Jacq.) root system. *Plant and Soil*, 189, 33–48.

Kallarackal, J., Jeyakumar, P. and George, S. J. (2004). Water use of irrigated oil palm at three different arid locations in Peninsular India. *Journal of Oil Palm Research*, 16, 45–53.

Kropff, M. J. (1993). Mechanisms of competition for light. In M. J. Kropff and H. H. van Laar (Eds.), *Modelling crop-weed interactions* (pp. 33–61). Wallingford, UK: CAB International (in association with International Rice Research Institute).

Kustas, W. P. and Daughtry, C. S. T. (1990). Estimation of the soil heat flux/net radiation ratio from spectral data. *Agriculture and Forest Meteorology*, 49, 205–23.

Kustas, W. P. and Norman, J. M. (1999). Evaluation of soil and vegetation heat flux predictions using a simple two-source model with radiometric temperatures for partial canopy cover. *Agricultural and Forest Meteorology*, 94, 13–29.

Kwan, B. K. W. (1994). *The Effect of Planting Density on the First Fifteen Years of Growth and Yield of Oil Palm in Sabah*. Technical Bulletin No. 11. Kota Kinabalu, Malaysia: Department of Agriculture, Sabah.

Liu, B. Y. and Jordan, R. C. (1960). The interrelationship and characteristic distribution of direct, diffuse, and total solar radiation. *Solar Energy*, 4, 1–19.

Long, S. P. and Bernacchi, C. J. (2003). Gas exchange measurements, what can they tell us about the underlying limitations to photosynthesis? Procedures and sources of error. *Journal of Experimental Botany*, 54, 2393–2401.

Lubis, M. E. S. (2016). *Water Dynamics and Groundwater Quality Assessment in an Oil Palm Ecosystem*. Ph.D. dissertation. Serdang, Malaysia: Universiti Putra Malaysia.

Massman, W. J. (1987). A comparative study of some mathematical models of the mean wind structure and aerodynamic drag of plant canopies. *Boundary-Layer Meteorology*, 40, 179–97.

Massman, W. J. (1997). An analytical one-dimensional model of momentum transfer by vegetation of arbitrary structure. *Boundary-Layer Meteorology*, 83, 407–21.

Miyazaki, T. (2005). *Water Flow in Soils*. Boca Raton, FL: CRC Press.

Mohd. Desa, M. N. and Rakhecha, P. R. (2006). Deriving the highest persisting monthly 24-hour dew points in Malaysia for the estimation of PMP. In S. Demuth, A. Gustard, E. Planos, F. Scatena and E. Servat (Eds.), *Climate Variability and Change-Hydrological Impacts. Proceedings of the Fifth FRIEND World Conference held at Havana, Cuba, November 2006. IAHS Publ. 308* (pp. 287–93). Wallingford, UK: International Association of Hydrological Sciences (IAHS).

Monteith, J. L. (1965). Evaporation and the environment. *Symposium of the Society of Experimental Biology*, 19, 205–34.

Monteith, J. L. (1973). *Principles of Environmental Physics*. London, UK: Edward Arnold.

Nelson, P. N., Banabas, M., Scotter, D.R. and Webb, M. J. (2006). Using soil water depletion to measure spatial distribution of root activity in oil palm (*Elaeis guineensis* Jacq.) plantations. *Plant Soil*, 286, 109–21.

Nikolov, N. and Zeller, K .F. (2003). Modeling coupled interactions of carbon, water, and ozone exchange between terrestrial ecosystems and the atmosphere. I: Model description. *Environmental Pollution*, 124, 231–46.

Paterson, R. R. M., Kumar, L., Taylor, S. and Lima, N. (2015). Future climate effects on suitability for growth of oil palms in Malaysia and Indonesia. *Scientific Reports*, 5, 1–11.

Rao, V., Rajanaidu, N., Kushairi, A. and Jalani, S. (1992). Density effect in the oil palm. In *Proceedings in the ISOP International Workshop of Yield Potential in the Oil Palm* (pp. 71–9). Bangi, Malaysia: International Society for Oil Palm Breeders and PORIM.

Rey, H., Quencez, P., Dufrêne, E. and Dubos, B. (1998). Oil palm water profiles and water supplies in Côte d'Ivoire. *Plantations, Recherche, Développement*, 5, 47–57.

Saxton, K. E. and Rawls, W. J. (2006). Soil water characteristic estimates by texture and organic matter for hydrologic solutions. *Soil Science Society of America Journal*, 70, 1569–78.

Sharkey, T. D. (2015). What gas exchange data can tell us. *Plant, Cell & Environment*, 39, 1161–3.

Sharkey, T. D., Bernacchi, C. J., Farquhar, G. D. and Singsaas, E. L. (2007). Fitting photosynthetic carbon dioxide response curves for C3 leaves. *Plant, Cell and Environment*, 30, 1035–40.

Shen, L. and Chen, Z. (2007). Critical review of the impact of tortuosity on diffusion. *Chemical Engineering Science*, 62, 3748–55.

Shuttleworth, W. J. and Wallace J. S. (1985). Evaporation from sparse crops - an energy combination theory. *Quarterly Journal of the Royal Meteorological Society*, 111, 839–55.

Skillman, J. B. (2008). Quantum yield variation across the three pathways of photosynthesis: Not yet out of the dark. *Journal of Experimental Botany*, 59, 1647–61.

Sopian, K., Hj. Othman, M. Y. and Wirsat, A. (1995). Data bank. The wind energy potential of Malaysia. *Renewable Energy*, 6, 1005–16.

Su, Z., Schmugge, T., Kustas, W. and Massman, W. (2001). An evaluation of two models for estimation of the roughness height for heat transfer between the land surface and the atmosphere. *Journal of Applied Meteorology*, 40, 1933–51.

Szeicz, G. and Long, I. F. (1969). Surface resistance of crop canopies. *Water Resources Research*, 5, 622–33.

Tan, Y. P. and Ng, S. K. (1977). Spacing for oil palms on coastal clays in Peninsular Malaysia. In D. A. Earp and W. Newall (Eds.), *International Developments in Oil Palm. Proceedings of the*

Malaysian International Agricultural Oil Palm Conference (pp. 183–91). Kuala Lumpur, Malaysia: Incorporated Society of Planters.

Teh, C. B. S. (2006). *Introduction to Mathematical Modeling of Crop Growth: How the Equations are Derived and Assembled into a Computer Program*. Boca Raton, FL: Brown Walker Press.

Thornley, J. H. M. (1970). Respiration, growth and maintenance in plants. *Nature*, 227, 304–5.

van Keulen, H. and Seligman, N. G. (1987). *Simulation of Water use, Nitrogen and Growth of a Spring wheat Crop*. Simulation Monographs. Wageningen, The Netherlands: Pudoc.

van Kraalingen, D. W. G. (1985). *Simulation of Oil Palm Growth and Yield*. Ph.D. thesis. Wageningen, The Netherlands: Wageningen Agricultural University.

van Kraalingen, D. W. G., Breure, C. J. and Spitters, C. J. T. (1989). Simulation of oil palm growth and yield. *Agricultural and Forest Meteorology*, 46, 227–44.

van Noordwijk, M., Lusiana, B., Khasanah, N. and Mulia, R. (2011). WaNuLCAS 4.0: Background on a model of water, nutrient, and light capture in agroforestry systems. Bogor, Indonesia: World Agroforestry Centre (ICRAF).

Wilkerson, G. G., Jones, J. W., Boote, K. J., Ingram, K. T. and Mishoe, J. W. (1983). Modeling soybean growth for crop management. *Transactions of the ASAE*, 26, 63–73.

Willmott C. J., Robeson S. M. and Matsuura, K. (2012). A refined index of model performance. *International Journal of Climatology*, 32, 2088–94.

Yin, X. and van Laar, H. H. (2005). *Crop Systems Dynamics. An Ecophysiological Simulation Model for Genotype-by-environment Interactions*. Wageningen, The Netherlands: Wageningen Academic Publishers.

Yu, S., Eder, B., Dennis, R., Chu, S. -H. and Schwartz, S. E. (2006). New unbiased symmetric metrics for evaluation of air quality models. *Atmospheric Science Letters*, 7, 26–34.

Zulkifli, Y., Geoffery, J., Saw, A. L. and Norul, S. T. (2006). Preliminary study on throughfall spatial variability and stemflow characteristics under oil palm catchment. In *Proceedings of the National Water Conference (in CD)*. Kuala Lumpur, Malaysia: Malaysian Hydrological Society.